Centre for Geo-Information

Thesis Report GIRS-2005-23

LEAF AREA INDEX ESTIMATION FOR NORWAY SPRUCE FOREST STAND BY MEANS OF RADIATIVE TRANSFER MODELLING AND IMAGING SPECTROSCOPY

Lucie Homolová

June 2005

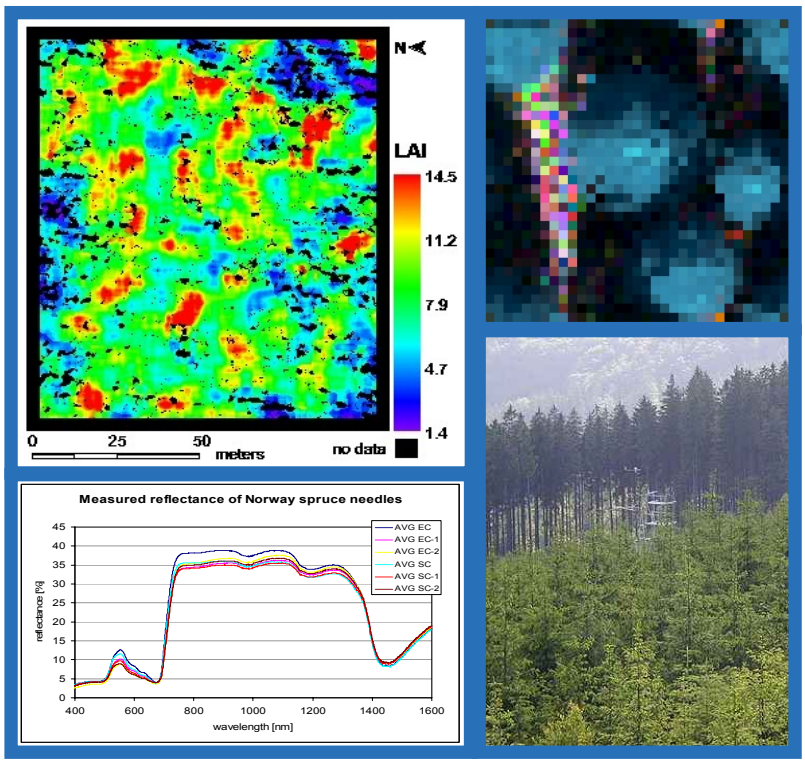

WAGENINGEN UNIVERSITY
WAGENINGEN UR

Leaf area index estimation for Norway spruce forest stand by means of radiative transfer modelling and imaging spectroscopy

Lucie Homolová

Registration number 81 07 19 357 110

Supervisors:

Zbyněk Malenovský
Prof. dr. Michael E. Schaepman

A thesis submitted in partial fulfillment of the degree of Master of Science at Wageningen University and Research Centre, The Netherlands.

June, 2005
Wageningen, The Netherlands

Thesis code number: GRS-80436
Wageningen University and Research Centre
Laboratory of Geo-Information Science and Remote Sensing
Thesis Report: GIRS-2005-23

Abstract

The main objective of the study was to evaluate and compare performances of two selected inversion techniques, and to explore the capability of the AISA image to estimate LAI of a young Norway spruce (*Picea abies* (L.) Karst) forest stand at the Beskydy Mts. (Czech Republic). A NADIR AISA hyperspectral image of very high spatial resolution (0.4 m pixel size) was used to retrieve the forest stand leaf area index. A 3-D radiative transfer model (DART) was appropriately parameterized to generate the spectral look-up table database, which was inverted by means of two inversion techniques: i) minimization of a cost function and ii) neural networks approach.

The mean LAI value of the observed forest stand retrieved by the minimization approach was equal to 6.33, and retrieved by the neural network approach was equal to 6.17. Both values are reliable, in comparison with the literature sources, nevertheless, the comparison with ground measurements showed very low correlations. The root mean square error (RMSE) calculated between estimated and measured LAI was equal to 2.442 in case of the minimization by a cost function, and equal to 2.621 in case of neural network inversion. None of the inversion techniques was capable to estimate high (generally higher than 9) values of leaf area index from the AISA image accurately. Comparison of the results of selected inversion methods showed very high reciprocal correlations (R>0.98), which indicated their comparable performance.

Keywords: Leaf Area Index, Norway spruce, DART, AISA image

Acknowledgements

First of all, I am deeply indebted to my supervisors Zbyněk Malenovský and Prof. dr. Michael Schaepman for their advice and help related to retrieval of biophysical parameters from hyperspectral remote sensing data. I would particularly like to thank to Zbynek for the provision of the DART model source code and the input data, furthermore for his guidance through the research project and his continuous encouragement.

This study is a result of a contribution from different organizations. The research would not have been done without the field and airborne data, which were supplied by the Academy of Sciences of the Czech Republic. I would like to express my thanks namely to Dr. Radek Pokorny for providing us the ground measurements of leaf area index and ancillary field data. Special thanks go to Emmanuel Martin (CESBIO) for his kind help and advice concerning the DART model. I would like to thank to Raul Zurita (GIS and RS department of WUR) for helping us with Matlab programming.

I am indebted to the Schuurman Schimmel – van Outeren Stichting for providing me a financial support. Also my special thanks go to my family in the Czech Republic for their understanding, encouragement and financial help.

Last but not least a special word of appreciation to all my friends for their support, especially to all the crazy MGI students who make our time at Alterra more enjoyable and to my friends from “Banik!” for a nice time, not only here in Wageningen.

Table of content

List of tables

List of figures

Acronyms

AISA	Airborne Imagining Spectroradiometer
ASCR	The Academy of Sciences of the Czech Republic
ATCOR-4	Atmospheric / Topographic Correction for Airborne Imagery, version 4.0
BRDF	Bidirectional Reflectance Distribution Function
BRF	Bidirectional Reflectance Factor
c	current age class of needles (first age class)
c+1	needles of one year old (second age class)
c+2	needles of two years old (third age class)
c+3	needles of three years old (fourth age class)
CC	Canopy Closure
DART	Discrete Anisotropic Radiative Transfer model
DBH	Diameter at Breast Height (diameter of tree stem in the height of 1.3m)
FOV	Field Of View
FWHM	Full Width Half Maximum
GMT	Greenwich Mean Time
HDRF	Hemispherical Directional Reflectance Factor
LAD	Leaf Angle Distribution
LAI	Leaf Area Index
LA_t	Total leaf Area [m2]
LIBERTY	Leaf Incorporating Biochemistry Exhibiting Reflectance and Transmittance Yields
LUT	Look-up table
MLH	Maximum Likelihood (classification)
NIR	Near Infrared
NN	Neural Networks
PCA	Plant Canopy Analyzer
r	needles older than four years
RMSE	Root Mean Square Error
RT	Radiative Transfer
SAIL	light Scattering by Arbitrarily Inclined Leaves
SAM	Spectral Angle Mapper (classification)
SLA	Specific Leaf Area
SWIR	Short Wave Infra Red
u_f	leaf volume density [m^2/m^3]
VI	Vegetation Index
Ω	Clumping index

1. Introduction and research objective

Norway spruce (*Picea abies* (L.) Karst) is one of the most important tree species, growing mainly in North, East and Central Europe. Norway spruce is fast growing species and thus is often used for a timber production. Norway spruce is the most important production species of the Czech Republic, 53.5% of the total forested area was covered by Norway spruce forests in 2003 (Anonymous, 2004).

In the recent years a lot of research has been done to determine the causes of Norway spruce forest decline in Europe (Cape, Paterson et al., 1989; Herman, Smidt et al., 2001; Hruska, Cienciala, 2003). The forest decline is a complex process caused by the multiple stress factors (chronic and acute). Several biochemical and biophysical indicators can be related with the current health stage of forest stands. One of the essential biochemical indicators is the content of photosynthetic pigments (chlorophyll a + b), which can be attributed to overall fitness and greenness of the vegetation. Acute stress of the vegetation decreases the chlorophyll content which, cause changes in the optical properties of green leaves. This allows remote sensing methods to detect and classified the stressed vegetation by means of changes in chlorophyll concentration (Demarez, Gastellu-Etchegorry, 2000; Zarco-Tejada, Miller et al., 2004).

The most important biophysical parameter, describing the structure of vegetation canopies is leaf area index (LAI), which can be used as an indicator of tree defoliation (Hall, Hogg et al., 2003). Negative statistical relationship is expected between LAI and defoliation. The spatial and temporal variability of LAI values within forest ecosystems is influenced by many different factors (species composition, development stage, site condition and management practices). The above mentioned factors in combination with different methods of LAI assessments may therefore lead to a variety of LAI estimates of forest stands (Pokorny, 2002).

Extraction of biophysical parameters such as leaf area index using remote sensing data has been proposed in many studies. The methodological approach to derive biophysical parameters from remote sensing data can be basically divided into two groups: i) empirical approach based on vegetation indices and ii) physical approach based on radiative transfer modelling

Number of optical vegetation indices (VI) derived from multi or hyperspectral remote sensing data for estimation of leaf area index have been reported in literature (Chen, Cihlar, 1996; Colombo, Bellingeri et al., 2003; Haboudane, Miller et al., 2004). The major problems in the use of vegetation indices for estimation of biophysical parameters are: i) asymptotic trend of the relation LAI-VI preventing accurate LAI estimates, when leaf area index exceeds a certain value (Baret, Guyot, 1991) and ii) external effect of atmosphere, background reflectance and illumination geometry (Broge, Leblanc, 2001). An alternative to empirical relationships is a modelling approach based on theory of radiative transfer theory. In this approach an inversion

technique of a vegetation reflectance model may be used to estimate biophysical parameters such as leaf area index (Jacquemoud, Baret et al., 1995; Hu, Inannen et al., 2000; Kimes, Gastellu-Etchegorry et al., 2002; Fang, Liang, 2005).

The issues of spatial and spectral resolutions of remote sensing data used for the estimation of biophysical and biochemical parameters have been addressed by several authors. Treitz (1999) give the overview of the possible use of hyperspectral data for biophysical parameters estimation in forest ecosystems. The hyperspectral remote sensing data provide ancillary and more detailed spectral information than multispectral data, which could be the advantage when estimating LAI from RS data (Broge, Leblanc, 2001; Lee, 2004). The impact of the different coarser spatial resolutions of RS data on LAI retrieval was explored by Tian (2003). The use of the RS data of very high spatial resolution (around 1m pixel size) for the LAI estimations is discussed in Gascon (2004). Compared with pixels of images with coarser spatial resolutions (such as 20m), pixels of images with very high spatial resolution carry qualitatively different information, which is related to parts of landscape elements (e.g. trees, shrubs). In the same publication Gascon explains why traditional VI (such as NDVI) could not be used for LAI estimations from RS data of very high spatial resolutions. Thus a special interested has to be paid to these data, when estimating biophysical parameters.

Forests ecosystem is a complex three-dimensional structure varying largely in amount, orientation and architectural placement of the vegetative elements (e.g. leaves, branches). All these attributes cause high variability of canopy reflectance (Asner, 1998). Imaging spectroscopy in combination with radiative transfer modelling might be an appropriate tool to resolve and map the forest complexity. For instance a Discrete Anisotropic Radiative Transfer (DART) model (Gastellu-Etchegorry, Demarez et al., 1996) is capable to simulate radiative transfer within the three-dimensional scenes representing any spatial combinations of trees, soil and other forest ecosystem elements.

1.1. Research objectives

The main objective of this research is to evaluate and compare two recent inversion methods estimating LAI within a young Norway spruce forest using a radiative transfer modelling combined with an airborne hyperspectral image of a very high spatial resolution (0.4 meters of pixel size): i) minimization by a merit function, and ii) inversion by an artificial neural network.

The research hypothesis is that LAI can be estimated with reasonable accuracy from the airborne NADIR hyperspectral image by means of the radiative transfer modelling on the level of forest stand. Based on the above mentioned hypothesis the following research questions were set:

1/ How reliable are values of LAI retrieved from the airborne NADIR hyperspectral images using current methods of radiative transfer modelling?
2/ Can the NADIR hyperspectral data resolve the full range of the LAI values present within the studied forest stand?

3/ Which inversion method of LAI estimation at the forest stand level is performing better from the following aspects:
   a/ Accuracy: Which method is giving more accurate results?
   b/ Feasibility: Which method is more feasible considering input data, time and technical requirements?

A new version of the Discrete Anisotropic Radiative Transfer (DART) model, extended by new forest structural parameters, was used for LAI estimation. However, the primary focus of this study was not the evaluation of these new structural features.

1.2. Set-up of the report

Chapter 1 introduces a brief overview about a general background of the research. Main research objective and subsequent research questions of the study are defined in that section. In the second chapter a literature review is conducted in order to deeply understand the topic of leaf area index retrievals. The overview of several methods of leaf area index estimations, focusing on the physically based approaches using radiative transfers, is discussed. Common methods of field LAI measurements are briefly introduced in this chapter. Chapter 3 describes the methodology used in the study. Description of the study area, field and airborne data acquisition, DART parameterization, and set up of the LAI retrieving methods is given there. Chapter 4 provides an extensive summary of the achieved results, which are interpreted and discussed in following chapter 5. Final conclusions and recommendations are stated in the last chapter 6.

2. Literature review

2.1. Canopy structure

A Norway spruce crown is presented by a non-random and highly organized structure of needles. Needles are clumped along woody twigs into shoots (set of needles developed in the same year). The shoots are formed into branches which are assembling a tree crown. The crown architecture is determined by the genetic and environmental factors and the ontogeny of a tree. A tree goes through three phases of shoot formation during its life. The phases are called proleptic, regular and preventitious and they cause development of different shoot types (Gruber, 1994). In the vertical direction one can distinguish three functional parts of a spruce crown (Cudlin, Novotny et al., 2001).

The crown (canopy) architecture of Norway spruce trees changes during the development stages of trees and during the growing seasons. A few basic parameters are used to describe the structure of trees and/or canopy. The most frequent parameters are: leaf area index (LAI), leaf angle distribution (LAD), and leaf clumping index (Ω).

The leaf angle distribution describes the geometry of leaves. It is often referred to the probability density of the distribution of the leaf normals with respect to the upper hemisphere (Liang, 2004). Direct and indirect methods were developed to measure LAD and so several mathematical descriptions of LAD can be found in the literature (Kucharik, Norman et al., 1998; Liang, 2004; Weiss, 2004).

The leaf clumping index quantifies the effect of non-random distribution of foliage. It is an important parameter to correct the indirect optical field measurements of LAI. Chen (1996) separated the clumping index into two components: clumping of needles at the shoot level and clumping of shoots within branches and crowns. Similar approach to quantify the clumping of needles within a shoot is introduced by Stenberg (1996). According to Chen and Liu (2003) it is possible to derive clumping index from multi-angular optical remote sensing data.

The leaf area index is a dimensionless variable that is basically defined as the total one-sided area of photosynthetic tissue per unit ground surface area (Watson, 1974). This definition is fully applicable for broad-leaved vegetation, because both sides of broad leaves have the same area. The needles of coniferous trees may occur in a cylindrical or a hemi-cylindrical shape (Chen, Black, 1992), and the definition of LAI is not applicable. Thus several authors proposed adjusted definition of LAI, taking into account the irregular shape of leaves or needles. For instance Chen and Black (1992) suggested as a more appropriated definition of LAI for coniferous canopies: half of the total interception area per a unit ground surface area.

The leaf area index drives the microclimate of canopy, controls water interception, radiation extinction and gas exchange (Bréda, 2003), therefore, LAI is an important input parameter for the ecological and plant physiology models (Nikolov, Zeller, 2003),

2.2. Ground-based measurements of leaf area index

There are two main categories of the ground-based estimates of leaf area index: direct and indirect methods (see reviews of these methods in Jnockheere et al.(2004), Bréda (2003) and Gower et al. (1999)).

The direct methods involve a measurement of leaf area, which is usually measured on a sub-sample of leaves and related to dry leaf mass. This relation is used to up-scale the information to the unit of observation (e.g. whole tree, stand). The direct methods are usually the most accurate, but they have the disadvantage of being time-consuming. They provide the reference for the calibration or evaluation of indirect methods.

Indirect methods infer leaf area from observation of another variable. These methods are generally faster than direct methods and thus more suitable for extensive sampling. The indirect methods of LAI estimation in situ can be divided in two categories: contact LAI measurements (e.g. inclined point quadrats method (Wilson, 1960)) and non-contact measurements.

Non-contact indirect methods of LAI estimations can be based on the Beer-Lambert extinction law applied to plant canopies (Monsi, Saeki, 1953). The law express the attenuation of the radiation in a homogenous turbid medium, which can be described by equation (1)

$$I = I_0 * e^{(-k*LAI)} \quad (1)$$

where I_0 is the incident radiation, I is the radiation transmitted below canopy, k is the extinction coefficient and LAI is the leaf area index. LAI measuring devices, using the above mentioned principle, are for instance DEMON (CSIRO, Canberra, Australia) or ceptometer (Decagon Devices Inc., USA)

The second group of optical indirect methods is based on the probabilistic approach of foliage elements (or complementary gap fraction) distribution, size and arrangement within a canopy. LAI is calculated by an inversion of the exponential expression of the gap fraction:

$$P(\theta) = e^{-G(\theta,\alpha)LAI/\cos(\theta)} \quad (2)$$

where θ is the view zenith angle, α is the leaf angle, P(θ) is the gap fraction distribution and G(θ, α) is named the G-function and it corresponds to the fraction of foliage projected on the plane normal to the zenith direction. Available measuring devices are: LAI-2000 Plant Canopy Analyzer (Li-Cor, USA), TRAC (Tracing Radiation and Architecture of Canopies, Wave Engineering, Canada) and cameras equipped with hemispherical lens.

Most of indirect optical methods do not distinguish leaves from other plant elements such as stem and branches. Alternative terms for leaf area index have been proposed: vegetation area index (Fassnacht, Gower et al., 1994), effective leaf area index (Chen, Black, 1992). The main assumption of the optical indirect methods is the random distribution of the foliage within a canopy. Several papers compared performances of indirect methods of LAI estimations with direct methods (Chason, Baldocchi et al., 1991; Smith, Chen et al., 1993; Fassnacht, Gower et al., 1994). The papers concluded that indirect methods underestimated LAI compared with direct measurements. The main reason of this underestimation is the non-random distribution of foliar elements, expressed by the leaf clumping effect. (Chen, 1996)

- **LAI-2000 Plant Canopy Analyzer**

The LAI-2000 (Li-Cor Inc., Nebraska) measures the attenuation of diffuse sky radiation in blue part of spectra at five zenith angles simultaneously. A measurement with the LAI-2000 consists of the readings above and below canopy, in both cases the sensor is looking up the sky. Five values of canopy transmittance are calculated for each pair of readings. From transmittance at the zenith angles, the LAI-2000 calculates foliage amount (effective leaf area index) and foliage orientation (LI-COR, 1992).

The final product (effective leaf area index LAI_{ef}) obtained from the LAI-2000 has to be corrected for the effect of foliage clumpiness and effect of supportive woody materials, when measuring the leaf area index of for instance coniferous forest canopies. Following the Chen's methodology (1996), clumping index is a correction factor to convert LAI_{ef} to LAI_t.

$$LAI_t = LAI_{ef}/\Omega \quad (3)$$

The smaller the clumping index, the more clumped canopy is. By treating the shoots as a basic unit of foliage, clumping index can be separated into two compounds (eq. 4):

- element clumping index (Ω_E) quantifying the effect of foliage clumping at the scale larger than the shoot,
- needle-to-shoot area ratio (γ_E) for the foliage clumping within the shoots.

$$\Omega = \Omega_E / \gamma_E \quad (4)$$

The plant area index LAI_t is the sum of the leaf area index (LAI) and the wood area index (WAI) and therefore combining equations 3 and 4 the final equation for calculation of "true" leaf area index is:

$$LAI = (1 - \alpha)*LAI_{ef} \times \gamma_E / \Omega_E \quad (5)$$

$$\text{where } \alpha = WAI / LAI_t. \quad (6)$$

- **Hemispherical photographs**

Hemispherical canopy photography is a technique studying plant canopies via photographs acquired through a camera equipped by a hemispherical (fisheye) lens, providing an extreme angle of view (FOV = 180°). The photographs can be acquired from beneath the canopy (oriented up to the sky) or placed above the canopy looking

downward. A hemispherical photograph provides a permanent record about position, size, density and distribution of the canopy gaps.

Crucial problem of the hemispherical photography for LAI determination is the selection of the optimal brightness threshold in order to distinguish leaves from sky. Often occurring methodological errors have been discussed by Rich (1993). A series of software packages for hemispherical images processing have been developed: CAN-EYE (Baret, Weiss, 2004), Gap Light Analyzer (GLA: www.rem.sfu.ca/forestry/), or Hemiview (Delta-T Device).

2.3. Inversion methods used to estimate LAI from remote sensing data

Biophysical parameters, such as LAI, can be estimated from remote sensing data by means of two basic approaches: empirical and physical approach. The empirical approaches use the statistical relationship between a vegetation index and LAI. Many studies were carried out using different vegetation indexes to estimate LAI from remote sensing data.

Radiative transfer model inversion consists in adjusting the values of input canopy biophysical and biochemical variables **V** in such a way that the bidirectional reflectance distribution function (BRDF) simulated with the radiative transfer model **M** matches the best BRDF measured by a sensor **R**. The model **M** requires a set of n_{var} input variables and the corresponding measurement configuration **C** (such as sun illumination direction, observation angles and wavelengths) (Combal, Baret et al., 2002). Than

$$R = M(V,C) \quad (7)$$

where the uncertainty ε accounts for measurement and model uncertainties. The simplest way how to solve the equation 7 is to compute and store the graph of the function **M**(**V**,**C**). Different mechanisms are applied to find the modelled reflectance that resembles the measured reflectance most precisely.

Several algorithms solving the inverse problem can be found in the literature. The first method, so called look-up table (LUT) approach, is widely used in combination with different minimization techniques of different merit functions. An example of a merit function can be root mean square error used for instance by Ufer Gil (2004) to estimate the chlorophyll content by inversion of the DART model. Next minimization techniques are based on a quasi-Newton algorithm (QNT) (Meroni, Colombo et al., 2004) or a simplex method (Kimes, Gastellu-Etchegorry et al., 2002). The common problem of LUT based methods is the potential to obtain multiple solution of the model inversion, so called ill-posed problem (Combal, Baret et al., 2002). Artificial neural network (NN) is another inversion technique used for LAI estimation. Several studies compared performances of NN and merit function approach (Kimes, Gastellu-Etchegorry et al., 2002; Ufer Gil, 2004). In both cases NN method gives better estimates of LAI. A new approach of object based retrieval of biophysical canopy variables using NN and RT modelling was introduce by Atzberger (2004). The object based approach shows very promising improvement, especially for LAI estimates, than the pixel-based approach.

Finally, Fang and Liang (2003) introduced the genetic algorithm to optimize the merit function to estimate LAI of homogenous canopies.

2.4. Reflectance models using the theory of radiative transfer

The radiative transfer (RT) theory describes a path of solar emitted photons from the moment of their penetration into the atmosphere layers, through interactions with the Earth surface, up to the backward reflection and detection by a sensor.

Vegetation reflectance can be modelled either at canopy level or leaf level. The optical properties simulated at the leaf level are often coupled with canopy reflectance models (Jacquemoud, Baret et al., 1995; Dawson, Curran et al., 1999; Demarez, Gastellu-Etchegorry, 2000; Meroni, Colombo et al., 2004). A well known leaf reflectance model is PROSPECT (Jacquemoud, Baret, 1990), which is based on the so-called “plate model” developed by Allen at al. (1969). PROSPECT was developed for broadleaf canopies, whereas a LIBERTY model was designed for conifer needles (Dawson, Curran et al., 1998). Turbid medium model LEAFMOD (Ganapol, Johnson et al., 1999) is another model operating at the leaf level, based on Kubelka-Munk theory.

Depending on the complexity of a canopy representation, one-dimensional (1D) or three-dimensional (3D) canopy reflectance models can be differentiated. The vegetation canopy of a 1D RT model is assumed to be a turbid medium with randomly distributed leaf clumps and gaps in between. SAIL model developed by Verhoef (1984) is an example of 1D RT model. In case of horizontally heterogeneous canopies, such as row crops or forests, the turbid medium analogy is not applicable. Thus Kimes and Kirchner (1982) developed a first RT model handling heterogeneity within vegetation canopies. Gastellu-Etchegorry et al. (1996; 2004) extended this model into 3-D Discrete Anisotropic Radiative Transferm (DART) model. Kuusk has designed so-called Markov canopy reflectance model, based on Markov chain theory. Gobron et al. (1997) developed a semi discrete RT model, and Goel and Grier (1986) introduced a hybrid 2-D model for row-planted vegetation, later extended into three-dimensional model (Goel, Grier, 1988). Basically there are two solutions to calculate canopy directional reflectance: numerical and approximate. For an extensive overview of possible solutions of canopy radiative transfer equations see Liang (2004).

Beside 3-D radiative transfer modes, which are the most suitable for dense vegetation canopies, the geometric optical models and computer models were introduced. Geometric optical models are more suitable for sparse canopies with regular pattern. The most of the canopy geometric optical models have been evaluated in the review of Chen (2000). The computer models provide the simulation of radiation regime over a complex canopy configuration using two methods: ray tracing and radiosity method. Ray tracing methods are based on sampling the photon trajectories within a canopy adopting so called Monte Carlo (MC) method. Alternative to the MC ray tracing method is a method of radiosity (Borel, Gerstl et al., 1991), which describes the amount of total energy leaving a surface per unit time per unit area (flux density).

- **DART**

DART (discrete anisotropic radiative transfer) is a 3-D model simulating bidirectional reflectance distribution function (BRDF) of a heterogeneous scenes. The model is using a similar approach as model proposed by Kimes and Kirchner (1982), which was based on the discrete ordinance method and iterative approach, but trying to avoid the main drawbacks of that model (Gastellu-Etchegorry, Demarez et al., 1996).

The 3-D scene is represented by the matrix of cells, which do not require the equal dimensions of cells. Cells are identified by x, y, z coordinates of theirs centers. Considering the information content of the cells, they are simulated as the turbid media (e.g. leaves, grass, trunks) or the solid media (e.g. soil, water). Each of them requires specific optical and structural characteristics.

The DART model processes the interactions of all source vectors of radiation within connected cells of the scene. Interaction mechanism depends on the cell type based on the structural and optical properties of different elements defined within a cell. The source vectors are transmitted through the gaps, totally intercepted by opaque cells and partly intercepted and transmitted by semi-opaque cells. Intercepted radiation gives rise to absorption or scattering mechanisms. Each cell, where scattering occurs, becomes a secondary radiation source. All direct solar source vectors, produced during the first radiative transfer iteration, are processed till they are totally absorbed and scattered, or till they reached a threshold value. In the second iteration all source vectors originates from secondary vectors and atmospheric source vectors are processed. The iterations are systematically done for all sources and for all directions. Once all source vectors have been processed, directional reflectance factors are computed for all upper cells of the scene.

The 1996 version of DART was successfully validated against field reflectance measurements (Gastellu-Etchegorry, Guillevic et al., 1999) and in frame of the RAMI exercise (Pinty, Gobron et al., 2000), where DART was compared with other 3-D RT models. The DART simulations showed consistent results in the visible part of spectra, however in the NIR part significant differences appeared. Based on first RAMI exercise three major approximations were successfully improved without increasing computation time (Gastellu-Etchegorry, Martin et al., 2004).

The last DART model version (2005) introduces several new structural features describing the growing strategy of the trees in more realistic way. The implemented improvements, based on a growing pattern of Norway spruce tree, are as follows (Malenovsky, Martin et al., 2003):

- vertical variability of leaf volume density,
- horizontal variability of leaf volume density and air cells,
- inconstant optical properties of leaves in vertical direction,
- variable stem diameter in vertical direction,
- direct simulation of branches of the first order, and
- simulation of twigs around the branches of the first order.

3. Material and methods

3.1. Methodological conceptual model

The general working methodology of the proposed study followed the schema indicated by a conceptual model in figure 1. First, the field data, acquired during the field campaign in the Beskydy Mts., was pre-processed. The DART model was used to simulate radiative transfer of the pre-prepared forest scenes. Their spectral signatures were stored in look-up tables (LUT), which were subsequently inverted for LAI estimation. Two different methodological approaches of inversion were applied: i) Minimizing merit function, and ii) Neural network approach. Verification of retrieved LAI values was done by direct comparison with ground truth data (measurements of LAI in the field). Finally, statistical analyses were carried out to validate the performance capabilities of both inversion methods.

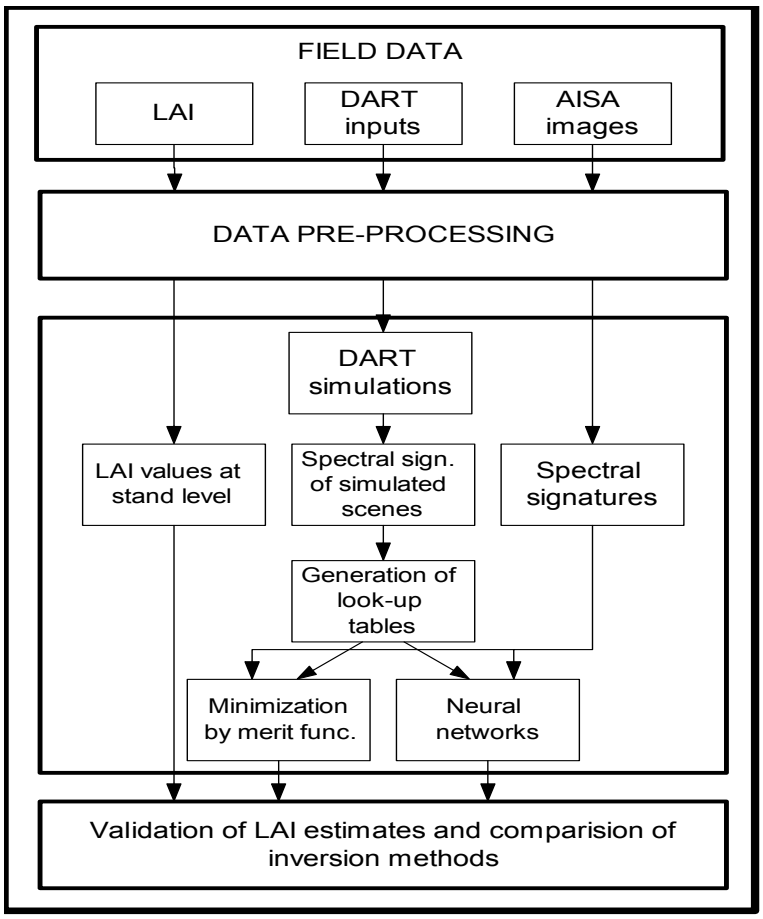

Figure 1. Conceptual model explaining a general working methodology.

3.2. Study area

The study area, called Bílý Kříž, is located in the Moravskoslezke Beskydy Mts., the eastern part of the Czech Republic at the borders with Slovakia (18.53863°E, 49.50256°N, 936 m a.s.l.) (see figure 2) The locality Bílý Kříž is an experimental study area of the Academy of Sciences of the Czech Republic (ASCR).

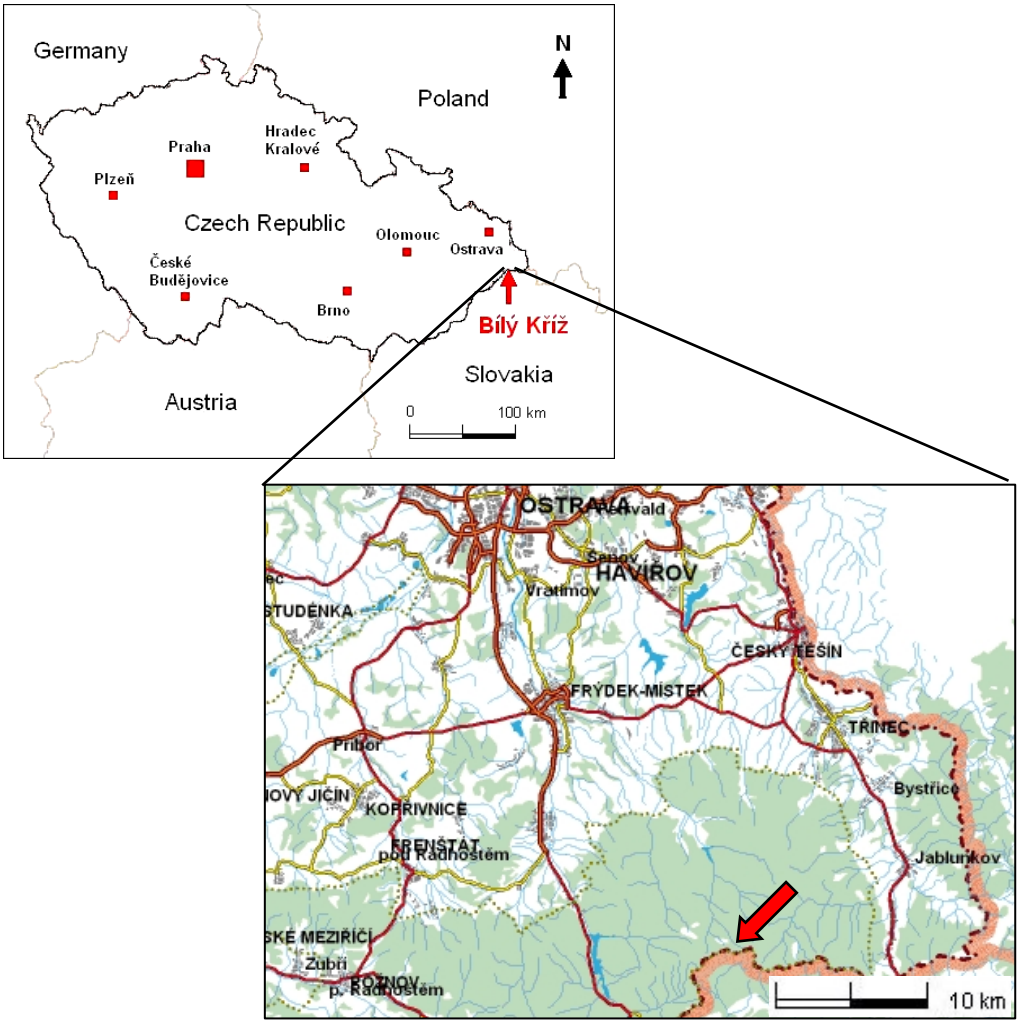

Figure 2. Location of the study area Bílý Kříž and Kykulka.

The geological bedrock of the area is sandstone from the Mezosoic era. The soil type is the humic podzol soil combined with the loamy sand soil. The depth of humic horizon is 60-80 cm with the gravel fraction of 30-40% and clay fraction of 15-38%. The average annual air temperature is about 5.5 ºC, the average annual precipitation amount is between 1000 and 1400 mm. The mean number of days with snow cover is 160 days per year. The average slope gradient of the study site is 13% with the slope oriented towards south-south-west (SSW).

The studied young forest stand is the experimental forest stand periodically monitored by the Laboratory of Ecological Physiology, Institute of Landscape Ecology, (ASCR). The forest stand represents the corridor plantation of Norway spruce (*Picea Abies*, (L.) Karst.) trees established in the regular spacing 2x1 m in 1981. The monoculture is

currently 27 years old with the average tree height of 10.6 m, and average diameter at breast height (DBH) of 12.8 cm. Several tending treatments were applied to reduce increasing forest stand density during last few growing periods. Two parts of two different tree densities were differentiated within the forest stands. The denser part of the forest contains currently 2044 trees/ha, the sparse one contains about 1362 trees/ha.

Second area involved in this study, called “Kykulka”, is located 11 km to NW from Bílý Kříž. At that secondary site eight mature Norway spruce trees, two trees representing one of four long-term stress response categories (Cudlin, Novotny et al., 2001), were selected for purpose of branch destructive sampling.

3.3. Field data and data processing

The field data were acquired in frame of a complex field/flight campaign carried out during August and September 2004 at the locations of Bílý Kříž and Kykulka. Ancillary ground data concerning the young forest stand were requested from the Institute of Landscape Ecology, ASCR. These data were used mainly for an appropriate parameterization of the DART model and for the validation purposes.

3.3.1. Canopy structural parameters of sample trees

Structural parameters of matured and young sample trees were mapped in order to describe the architecture of Norway spruce crowns and stand canopies. Automatic mapping was done by the laser rangefinder Impulse 200 and an electronic compass MapStar combined with the FieldMap software (IFER, 2004).

Following parameters were measured within the mature forest stand: position of the trees (X, Y coordinates), DBH, height of the trees, height of the live and death part of crowns, and ground projection of the crowns (at least 8 points were needed to determine the perimeter of the crowns).

Only two parameters were measured for 16 sample trees of the young forest stand: position of the trees (X, Y coordinates), and DBH. Other required structural parameters of the young trees were provided by Dr. Radek Pokorny from the Institute of Landscape Ecology (ASCR) acquired during his continual research of Norway spruce physiology.

3.3.2. Destructive measurements of branch samples

Destructive measurements were carried out to obtain following structural parameters: i) the ratio of needle age classes, ii) horizontal distribution of leaf density from a branch base towards crown periphery, and iii) the foliage clumping index. Eight mature trees were selected for the purpose of destructive sampling at the second study site Kykulka. One representative branch of first order was collected from each functional crown part (i.e. juvenile, productive, saturation part (Cudlin, Novotny et al., 2001)). The positioning within a crown and dimensions of each branch were measured directly in the field. The

collected branches were immediately transported into the laboratory for further processing. The methodology of subsequent analyses was as following:

- Each branch was divided into several segments approximately 60 cm long for branches from production and saturation crown part, and approximately 40 cm long for branches of juvenile crown part. The final length of the segments was depending on the overall length and shape of the branch.
- Length, depth and diameter of woody part at the base and the top of each segment were measured. The percentage ratio of needle age classes (current year (c), one year old (c+1), two years old (c+2), three years old (c+3) and the rest age classes (r)) was calculated.
- Ten representative shoots were selected based on the distribution of needle age classes from each segment and analyzed in following manner:
    - shoots were scanned on a desktop double lamp scanner in a very fine resolution of 600 dpi in true colors to get their projected area,
    - scanned shoots were dipped into liquid nitrogen and all the needles were pruned away from a woody twig,
    - the remaining woody twigs were again scanned to get their projected area,
    - and the separate needles were also scanned to obtain their projected area,
    - finally, the needles and twigs were dried in a laboratory oven (60°C, 48 hours), and weighted to obtain their dry mass.
- The remaining shoots of each segment were placed in dark dry condition and the dry weight of needles and twigs were determined after two months. The woody parts of branches with diameter larger than 1 cm were analyzed separately. Their diameters at both ends and total length were measured and total wood volume was computed.
- The projected needle area obtained from the representative shoot analyses was scaled up to the branch segment level by means of the specific leaf area ratio (SLA [cm^2/g] = projection area of fresh needles [cm^2] / dry biomass of the needles [g]).

3.3.3. Leaf area index field measurement

The real values of leaf area index were measured in field by two indirect optically-based methods using: i) the Li-cor LAI-2000 Plant Canopy Analyzer (PCA), and ii) a digital camera with a hemispherical lens. The sampling scheme within the young forest stand followed the regular pattern of three parallel transect lines placed in the east-west direction, each of 14 points. The sampling points were distributed regularly in the pattern of 5x3 m.

- **PCA LAI-2000**

The measurements and further processing of the data were conducted by Dr. Radek Pokorny from the ASCR. Due to the time constrains, the measurements were taken only for the sample points of the middle transect. The complete transect measurement was repeated twice, always under the diffuse radiation conditions. The field of view (FOV) of the optical device was restricted to zenithal angle of 43°, masking fourth and fifth ring of detectors. A view cap restricting azimuthal view angle from 360° to 270° was used to remove an operator from the sensor FOV. The values of an effective leaf

area index per each point were calculated using the software utility called comma.exe (LI-COR, 1992). The effective LAI values had to be corrected from the effect of leaf clumpiness and effect of supportive wood in order to get the real values of leaf area index. The coefficient to correct the effective LAI to "true" values was obtained from the destructive and PCA-2000 measurements conducted within the same forest stand during growing period 1997 (Pokorny, Marek, 2000; Pokorny, 2002). The ratio computed between the LAI resulted from the destructive measurements and LAI_{ef} gained from PCA LAI-2000 measurements was considered as the clumping correction coefficient of the leaves and woody parts.

- **Hemispherical photographs**

Hemispherical photographs were taken with digital camera Nikon Coolpix 8700 with the fish-eye lens, offering the FOV of 180º. For each sampling point set of 6 images were taken (one upward and one downward looking image (see figure 3) and four images of oblique views (at zenith angle 57.5°). The images were first enhanced using the Adobe Photoshop software in order to eliminate differences in illumination condition during acquisition of the photographs. A neural based software called CAN-EYE (Baret, Weiss, 2004) was used for a further processing. Currently CAN-EYE is able to handle only upwards and downwards looking images from which calculates one value of leaf area index per plot and for each image the effective leaf area index (LAI_{ef}) is given. The images were first sorted into the groups representing subplots of 3x3 sampling points and all nine images of such a subplot were processed together in CAN-EYE. The essential and most sensitive step in the whole processing procedure was the classification of images. The images were interactively classified into two classes: i) sky or soil in case of downward looking images, and ii) leaves. Based on the classification the average gap fraction was derived end effective and the "true" LAI and clumping index were calculated.

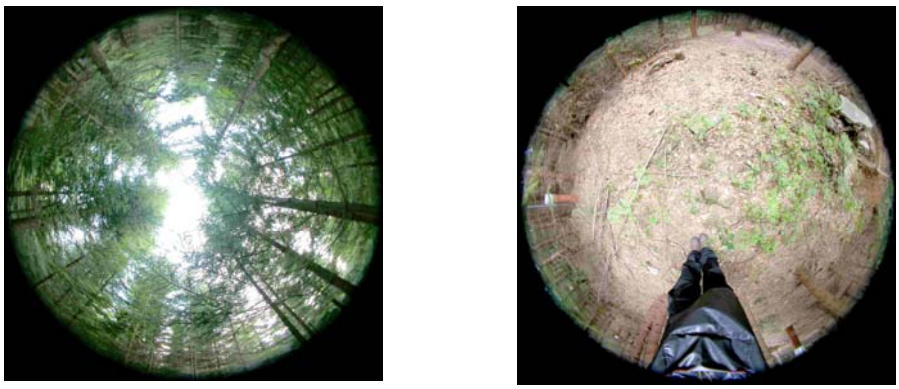

Figure 3. Example of the upward looking (left) and downward looking (right) hemispherical photograph taken for the field determination of leaf area index.

3.3.4. Optical properties of needles and background elements.

The directional hemispherical reflectance and transmittance of spruce needles and background elements (spruce bark, leaves of understory species like black-berry, beech, mountain ash, etc.) were measured by field spectrometer ASD FieldSpec Pro combined with Li-Cor integrating sphere Li 1800-12. The spectral range of measured data was between 350-2500 nm with the step of 1 nm. The representative samples of three needle age classes (c, c+1, c+2) were taken from sunlit part (3rd whorl) and shaded part (7th whorl, inside a crown) of ten sample trees selected within the young forest stand. The method proposed by Daughtry (1989) and extended by Mesarch et al. (1999) was adapted for reflectance and transmittance measurements of the Norway spruce needles (Malenovský, Cudlín et al., submitted).

The optical properties of study site background elements (soil, senescent needles) and spruce bark were measured with Li-Cor spectroradiometer Li-1800 and integrating sphere Li 1800-12 during the field campaign at Sumava Mts. in September 2003 (Ufer Gil, 2004).

3.4. AISA hyperspectral images acquisition and post-processing

The airborne hyperspectral images were acquired by the AISA Eagle (Airborne Imagining Spectroradiometer) sensor. AISA Eagle is a pushbroom system equipped by a CCD matrix of 1024 spatial pixels and 512 active spectral pixels, operating within the spectral range of 400 – 970 nm. The sensor is capable to acquire any spectral band combination up to datasets of 244 bands (SPECIM, 2004). The final spatial and spectral resolution of the acquired images is related to the flight properties (i.e. altitude of the plane, speed of flight) and a sensor set-up (e.g. focal length of fore optics) (see table 1). A set of NADIR hyperspectral images of very high spatial resolution (0.4m) was acquired over the study area “Bílý Kříž” at September 18th 2004.

Table 1. Parameters of the flight set-up for flight campaign over the study area “Bílý Kříž” (September 18th 2004).

Parameters	
Spatial resolution /Ground pixel size [m]	0.4
Band widths [nm]	8.6-10,0
Number of bands	64
Flight speed [m/s]	50
FPS (Frames per second)	125
Swath width [m]	204.8
Altitude [m]	384
Focal length of lens [mm]	23
FOV (Field of view) [º]	29.9
Binning of pixels (spectral x spatial)	8x2

3.4.1. Radiometric calibration

The radiometric calibration is a process that converts sensor recorded digital numbers (DN) to the values of radiance [uW/cm^2 sr nm].

The radiometric corrections of the AISA image were performed using a special software CaliGeo, compatible with ENVI standard format, designed and provided for the AISA sensor by the SPECIM company (SPECIM, 2004). The sensor calibration coefficients used for the radiometric correction, were measured in laboratory by SPECIM, using an integration sphere and an illumination source of known light intensity.

3.4.2. Atmospheric correction

The atmospheric correction of the AISA image, converting the radiance values into the reflectance values, was done using the Empirical Line approach. This method requires selection of at least one calibration target and its reflectance signature measured in the field during the same time as an image acquisition (under the same illumination conditions). The correction uses a constant gain and offset for each band to perform the best fit between measured spectra and image spectra of the same ground target and thus removing the atmospheric effects.

The set of five Lambertian surface calibration panels (each 2.5x2.5m large), with stable reflectance response from 5% to 60% in the color range from black to white, were placed on the flat ground. Their reflectance was measured by the field spectrometer (FieldSpec Pro) during the AISA image acquisition. The calibration panels were easily localized at the AISA image and Empirical Line approach was applied (ENVI software) using the ground spectra only of four of them (signal of the brightest panel was oversaturated at the AISA image, hence it was excluded from the correction procedure).

3.4.3. BRDF correction

The reflectance of surface covers depends on the viewing and sun illumination geometry, which is described by the bidirectional reflectance distribution function (BRDF). Due to the sensor view angle (FOV > 20º) the brightness gradient over an airborne image may occur with the increasing view angle. When scanning in the principal plane, the brightness effect is very strong in the hot spot. The BRDF effect occurs in the terrain with slopes facing to the sun and away from the sun. Therefore, the nadir normalization method was applied on the AISA reactance image using the ATCOR-4 tool (Richter, 2005) to exclude the BRDF influence.

3.4.4. AISA image classification

An area, containing the forest stand of interest was selected and cut out from the AISA image. The image subset was automatically classified to differentiate the shaded and sunlit part of crowns from the other ground surfaces, adopting an approach designed for very high spatial resolution imagery (Gascon, Gastellu-Etchegorry et al., 2004).

Two classification methods were applied and their performances compared by means of the error matrices and the best result was used for the LAI retrieval. Spectral angle mapper (SAM) (Kruse, Lefkoff et al., 1993), the first classification procedure applied to the AISA image, is a physically based spectral classification developed for a hyperspectral data. The algorithm determines the spectral similarity between two spectra by calculating the angle between the spectra, treating them as vectors in n-dimensional space (depends on the number of spectral bands). The spectral endmembers were derived from the regions of interest (ROI) in ENVI for each ground cover class. In order to improve the results of SAM classification the minimum noise fraction (MNF) transformation of the AISA image was performed. The MNF transformation consists of two cascaded principal component transformations and it is used to segregate noise from the data.

Maximum likelihood (MLH) classification was second approach used to classify the AISA image. MLH assumes that the distributions of points for each class in each band are normally distributed (Gaussian) and the algorithm calculates the probability that a given pixel belongs to a specific ground cover class (Lillesand, Kiefer, 2000). A high pass convolution filter (window size of 3x3 pixels) was applied to the AISA band no. 41 (764 nm) to enhance differences between sunlit part of crowns and shaded crowns. Resulting image was added as a pseudo-band to the initial AISA image to improve the MLH classification process.

3.5. Parameterization of the DART model

3.5.1. Directional parameters

The position of the sun over the research area was calculated for the particular location and exact time of the flight, which was September 18th, 2004 at 11:50 a.m. (GMT). The sun zenith angle (Θ) was equal to 47.8° and the sun azimuth angle (Φ) was equal to -3.5° (measured from South). Both angular parameters had to be transformed to fit the definition of sun zenith and azimuth angles in DART resulting in DART sun zenith angle of 183.5°, and DART sun azimuth angle of 137.8°.

3.5.2. Selection of spectral bands and RT parameters

The bands in red part of spectra are strongly influenced by the chlorophyll concentration of the needles. The leaf water content is influencing the wavelength from 800 nm. The canopy structure affects the reflectance at the NIR plateau (750 – 1000 nm) (Lillesand, Kiefer, 2000; Meer van der, Jong de, 2001). Unfortunately, the spectral information captured by the AISA sensor was found to be noisy for the wavelength higher than 900 nm. Based on this knowledge the suitable spectral bands for LAI retrieval were selected between 700 to 800 nm. The parameters of the selected spectral bands simulated by DART were according to the position of AISA bands (table 2). Four AISA bands were selected (band no. 37, 38, 40 and 42) for the RT simulations and building the look-up-table (LUT) database.

Table 2. Description of the AISA spectral bands selected for DART simulations.

Band No.	Band centre [nm]	FWHM
37	726.76	9.35
38	736.11	9.35
40	754.88	9.51
42	773.92	9.52

The multispectral mode of DART was used for RT simulations. Multiple scattering was simulated within ten iterations of radiative transfer and the output images were requested for each iteration. Due to the no changes in the albedo the simulations were stopped after sixth simulation. The Gauss-Seidel approach (Gastellu-Etchegorry, Demarez et al., 1996) was used to extrapolate the multiple scattered radiation in the last iteration.

3.5.3. Basic 3-D landscape representation

The DART model is working with the basic scene (also called maket or mock-up), which is a 3-D representation of a simulated landscape (figure 4). The forest landscape was created as a repetition of the basic pattern of four trees forming a rectangular cell matrix. The pixel size of the basic scene cell was set to be 0.2 m. The dimensions of the scenes varied with different canopy closures.

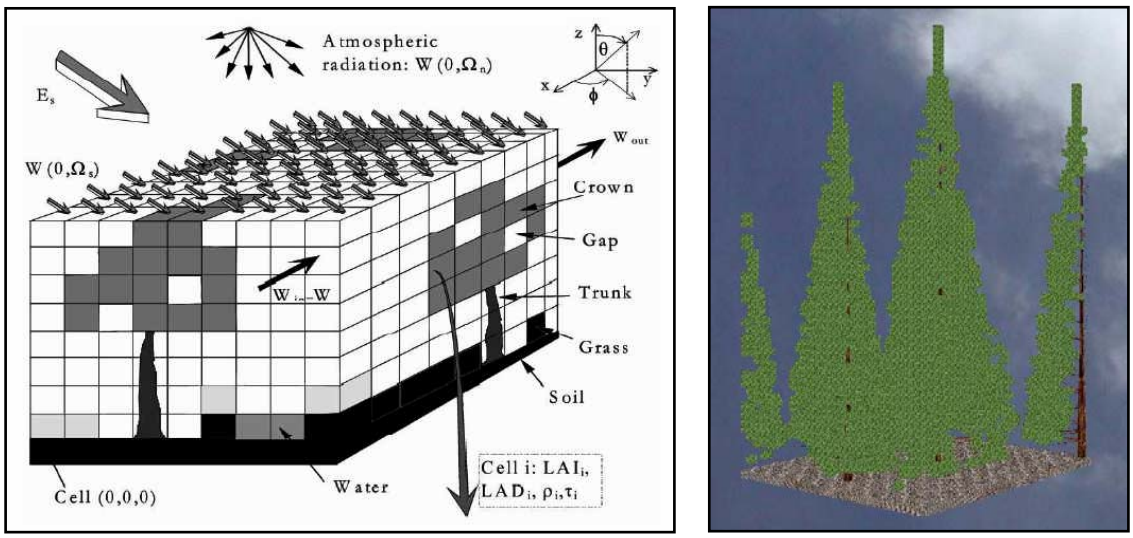

Figure 4. Representation of a cell matrix (left) and the visualisation of 55% canopy closure basic scene of spruce stand in DART (right)

3.5.4. Canopy closure of the simulated forest

Six categories of percentage of canopy closure (55%, 65%, 75%, 85%, 90% and 95%) were simulated in order to describe different densities of forest stands (figure 5). The selection of canopy closures categories was based on the exploration of the AISA image and preliminary calculation of possible canopy closures. The scene dimensions and spacing between trees (exact tree location) were linearly decreased with increasing canopy closure to achieve selected canopy closures in DART.

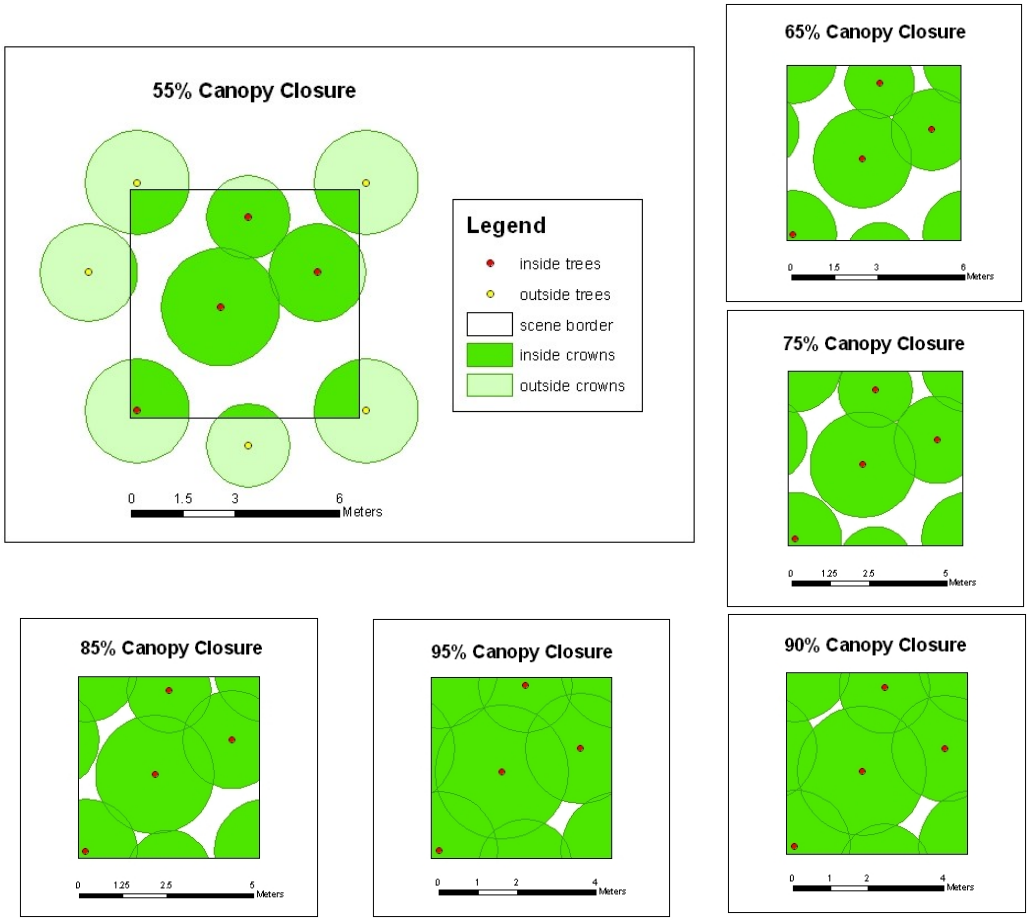

Figure 5. Schematic representation of six canopy closure categories used for building the spectral look-up tables (the legend of 55% CC is applicable for all canopy closures categories).

3.5.5. Tree structural and optical properties

A tree, used for the scene building, was defined by exact location (X, Y coordinates), and specific structural and/or optical parameters. Each tree was treated as one "DART tree species", which means that all input parameters could be defined separately for each species. One suppressed tree, one dominant and two average trees were defined within the scene. The basic allometric parameters (e.g. tree height, trunk diameter) were derived from the field measurements accomplished by the laser rangefinder Impulse 200 and FieldMap system, or from the direct measurements of the same forest stand provided by Dr. Radek Pokorny (ASCR).

- **Crown architecture**

Several geometric simplifications of tree crown shape are available in the DART model. The truncated cone with zero upper radius was used to represent the Norway spruce crowns in this study. The height of a live crown and the bottom radius of a crown were derived from the field destructive measurements in 1997 and the parameters were linearly recomputed to reflect the current growing stage of the young forest stand.

- **Crown vertical levels**

Any number of crown vertical levels can be defined by an operator within a simulated tree. Specific tree parameters (e.g. trunk diameter, distribution of leaf volume density and percentage of full leaf cells) can be defined per each level separately. Height of a tree levels has to be specified as a percentage of the total crown length, expressed as a relative value between 0 and 1. The total sum of relative heights' of tree levels must be smaller or equal to one. The number of tree levels was defined according to the height of crowns, i.e. 10 levels for the suppressed tree and 11 levels for the dominant and average tree.

- **Trunk definition**

Trunk height and diameters of each "DART tree species" are defined separately inside and outside a crown. The trunk height within a crown was specified 2 meters lower than length of the crown in order to avoid unrealistic influence of a trunk at the crown top. The trunk diameters were derived from the destructive measurements of the experimental forest stand in 1997, carried out on eleven specific trunk heights. A simple ratio DBH_{04}/DBH_{97}, where DBH_{04} is diameter at breast height (DBH) of the universal DART trees derived from the field measurements, and DBH_{97} is an average measured DBH, was used to compute trunk diameters at the same tree heights as measured in 1997. Finally, a statistical exponential function was applied to calculate a trunk diameter at any tree height for each "DART tree species" (see figure 6).

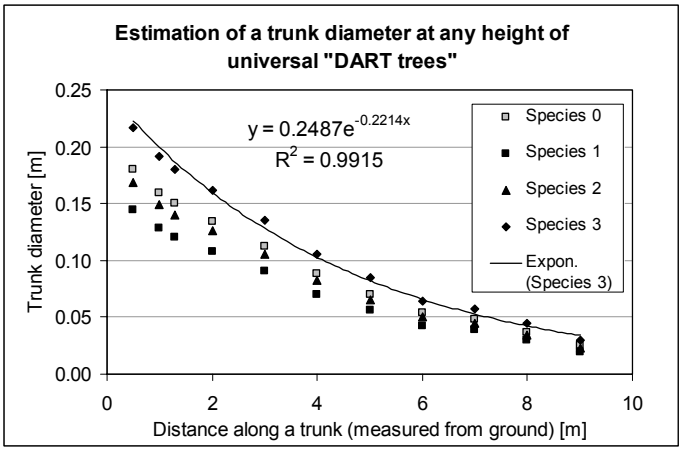

Figure 6. Estimation of the trunk diameters at any height of universal "DART tree species" (exponential function of species no. 3 is given).

- **Vertical distribution of leaf area within a crown**

The varying leaf distribution in the vertical direction is introduced in a new version of DART through the vertical weights of unit leaf volume density u_f [m^2/m^3]. The leaf volume density of a cell at any location can be described by the following equation:

$$u_f[j,x,y,z] = u_f[j].w[j,l].w[j,x(l),y(l)] \quad (8)$$

where $u_f[j,x,y,z]$ is leaf volume density of tree species **j** in particular location (x,y,z) and $u_f[j]$ is unit leaf volume density of tree species **j**. The vertical weight of u_f at tree level **l** of

tree species **j** is denoted as w[j,l] and w[j,x(l),y(l)] is horizontal weight of u_f, which is discussed in the next section.

The required vertical weights were generated from the vertical distribution of total leaf area for an average suppressed, co-dominant and dominant tree, obtained from the destructive measurements in 1997 (Pokorny, 2002). First, the total leaf area of four DART trees was estimated from an empirically derived linear equation 9. based on the crown surface area (Pokorny, 2002).

$$LA_t = 3.2010*C_a - 25.687 \quad (9)$$

where LA_t is total needle area in m^2 and C_a is crown surface area [m^2], which was derived from the simplified shape (cone) of spruce crown. The adjusted correlation coefficient (r^2) equal to 0.94 ensured statistical significance of the derived allometric linear relationship.

Percentage of total leaf area presented in each tree level was derived from the graphs of vertical distributions of total leaf area. The vertical weights of leaf area distribution were computed for each tree level as the ratio between unit leaf volume density of the whole tree and leaf volume density within each crown level.

- **Horizontal distribution of leaf area and empty cells**

Another structural feature of the last DART version allows to define varying leaf volume density also in the horizontal direction (parameters **α**, **β**, **γ** and **κ**) and to specify the horizontal distribution of full leaf and empty (air) cells (parameters **a** and **b**) within each tree level **l**. Function of the horizontal distribution of leaf volume density is indicated in figure 7.

The position of each leaf cell can be expressed as the relative ratio r(x,y,z)/Max r(x,y,z), where r(x,y,z) is current position of a leaf cell and Max r(x,y,z) is the position at the crown periphery. Depending on the horizontal parameters of leaf volume density α, β, γ and κ, specified for each crown level, the leaf volume density of each leaf cell is calculated in following manner:

- if ratio $\in \langle 0,\alpha)$ than $u_f[j,x,y,z] = 0$
- if ratio $\in \langle \alpha,\beta)$ than $u_f[j].w[j,l].w[j,x(l),y(l)]$, where w[j,x(l),y(l)] = (ratio–α)/(β-α)
- if ratio $\in \langle \beta,\gamma)$ than $u_f[j,x,y,z] = u_f[j].w[j,l]$
- if ratio $\in \langle \gamma,\kappa)$ than $u_f[j].w[j,l].w[j,x(l),y(l)]$, where w[j,x(l),y(l)] = (κ-ratio)/(κ- γ)
- if ratio $\in \langle \kappa,1\rangle$ than $u_f[j,x,y,z] = 0$

If the crown air spaces (empty cells) need to be defined, then two additional horizontal parameters **a** and **b** must be specified. These parameters determine zones of total (100%) inner and peripheral crown defoliation.

- if ratio $\in \langle 0,a)$ than 100% of empty cells is defined
- if ratio $\in \langle a,b)$ than percentage of leaf cells is specified by an operator
- if ratio $\in \langle b,1)$ than 100% of empty cells is defined

(The detailed explanation is given in the DART user manual.)

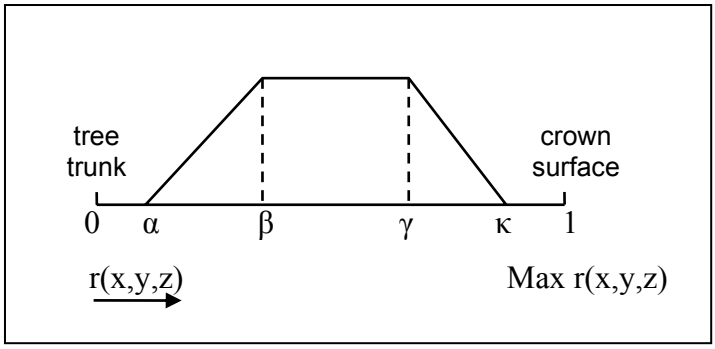

Figure 7. DART function for horizontal distribution of leaf volume density u_f [m^2/m^3].

It was assumed that parameters **κ** and **b** are equal to 1, which means that none peripheral crown defoliation was considered for the young trees. Parameter **α** was assumed to be equal zero. Based on those assumptions only parameters **β**, **γ** and **a** had to be determined.

Because the data describing the horizontal distribution of leaf area of the young trees were not available, the horizontal parameters were derived from the analyses of representative branches of mature Norway spruce trees, which were collected during the field campaign at Sumava Mts. in 2003 (Ufer Gil, 2004). Seven branches from juvenile crown part and five from productive part were used for mapping of the leaf horizontal distribution after exclusion of four non-representative branches. The juvenile branches of mature tree were considered to have similar horizontal distribution of leaf area as the branches at the upper crown half of young trees. The first productive branches of mature trees were considered to be similar to the lower branches of the young tree crowns.

The branches were divided into the regular segments (see section 3.3.2), and a digital photograph of each segment was taken in the laboratory. The boundaries of segments and holes within branches were digitized using ArcGIS software. The digitized branch segments were assembled into the whole branch with the initial point **O**[0,0] located at the beginning of each branch. The multiple buffer rings of 0.2 m were created around the initial point **O** with the distance corresponding to the dimension of a cell size defined in DART. The branch digital coverage was intersected with the buffer coverage and a sector of a circle occupied by a single branch was determined for each of the analysed branches (figure 8). It was assumed that the branches are not overlapping each other within a whorl and they are distributed evenly.

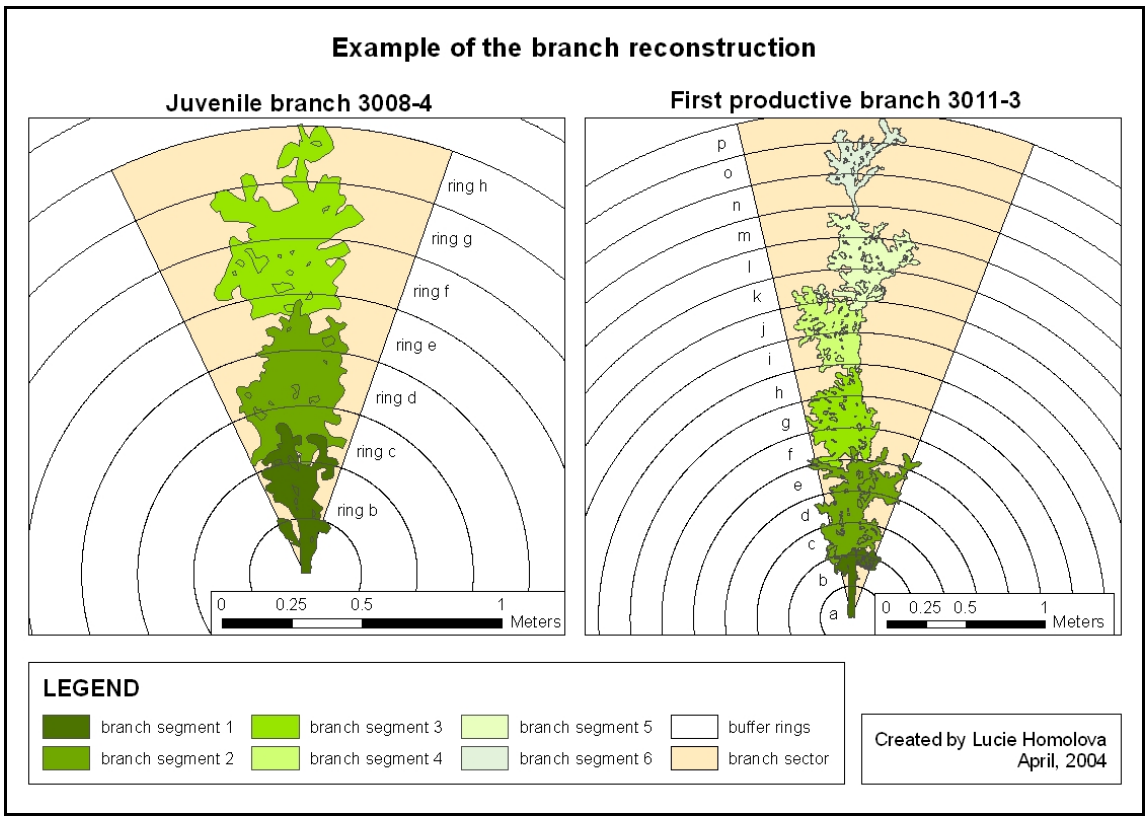

Figure 8. Example of the reconstruction of a juvenile (left) and 1st productive (right) branches.

1/ Horizontal structural parameters **β** and **γ** of leaf volume density

First of all percentage of total branch segment area per each sector ring was calculated. The same procedure of destructive branch analyses as described in chapter 3.3.2 was used during the field campaign in 2003. The result of the total needle area per segment was used to compute the total needle area [m^2] within each sector ring and in final step recomputed into the percentage of the half of total needle area per sector ring. The average values of these percentages for juvenile and first productive branches were plotted in cumulative way. The cumulative curve was fitted by a sigmoid function:

$$y = \frac{a}{1 + e^{-\frac{x-b}{c}}} \tag{10}$$

The first and second derivative of the sigmoid function was calculated. Finally, the parameter **β** was estimated as the maximum and the parameter **γ** as the minimum of the second derivative function.

2/ Horizontal parameter **a** of inner zone of defoliation

Only first productive branches were taken into account for calculation of the parameter **a**. The length of non-leaf part for each examined branch was determined, averaged and converted into the percentage of total branch length. The average value of non-leaf

length of a branch was considered to be representative for the bottom part of the tree crowns simulated in DART. The inner defoliation zone was not introduced for the juvenile part of DART crowns (last two crown levels). Radius of the defoliation inner zone was assumed to be horizontally linear, thus the radius values of inner defoliation zone were interpolated for any tree height using a linear equation.

3/ Percentage of full leaf cells

Percentage of the sector ring area occupied by the branch segments was first determined for each sector ring separately. Averaging these values over all sector rings gave a percentage of full leaf cells per one crown whorl. It was assumed that one crown level is occupied by two whorls, thus the final percentage value of full leaf cells had to be doubled. The analysis of 1st productive branches gave the value for the bottom part of crown and the juvenile branches gave the value at the middle of the young tree height. The values for tree levels in between were linearly extrapolated. The constant percentage as obtained from juvenile branches was defined for remaining upper crown levels, except 85% of full leaf cells for the last upper level and 80% for the second upper crown level.

- **Simulation of the first order branches**

Simulation of branches of the first order is next structural feature introduced in the new DART version. Each branch has to be defined by a relative height of its branch base on a trunk. The orientation of a branch is defined by its zenith and azimuth angle. In average two branch whorls per a crown level were created along the trunk each assembled from four to six branches. The branch zenith angle linearly decreased from 90° to 60° with growing tree height.

- **Tree optical properties**

The latest DART version allows specifying the optical properties of needles for each crown level separately. DART leaf optical properties were calculated as a weighted average of hemispherical optical characteristics of last three needle age classes of sunlit and shaded needles. The vertical distribution of needle age classes, expressed as percentage of c, c+1 and r needle age class, were obtained from destructive sampling within the same forest stand in 1997 (Pokorny, 2002). For the purpose of this study the vertical distribution of needle age classes was assumed to be comparable with situation in 1997. Seven zones of different optical properties (directional hemispherical reflectance and transmittance) were differentiated according to the relative tree heights. The optical properties of first three bottom zones were based only on the optical properties of shaded needles. The optical properties for transition middle zones were calculated as an average optical property of shaded and insolate needles, and last two upper zones were represented only by insolate needles.

The optical properties of woody elements, i.e. Norway spruce bark of branches and trunks, were measured during the field at Sumava Mts. in 2003.

3.5.6. Leaf area index in DART

The value of LAI can be specified as the leaf area index of a “DART” tree species related to the area of whole sub-scene or as a value expressing leaf volume density (u_f). The tree LAI was entered as a variable value of leaf volume density. Different combinations of leaf volume density and canopy closures led to the targeting values of leaf area index of the whole simulated scene, which was used to build the spectral look-up table database.

3.5.7. Background structural and optical properties

The ground cover of the young forest stand consists mainly of litter (senescent needles) and bare soil. There are not many understory species growing due to the lack of light. Therefore, the effect of understory vegetation was not impeached for the DART simulations. The final optical properties of the ground surface were calculated as a weighted value of the optical properties of bare soil (weight 0.5) and optical properties of senescent needles (weight 0.5).

3.6. Building of the spectral look-up table database

The combination of two free variables (canopy closure and leaf volume density) led to the different values of stand leaf area index per a simulated scene (see appendix 1). The look-up table (LUT) databases were build for each simulated canopy closure (55%, 65%, 75%, 85%, 90% and 95 %). In total 336 simulations were carried out to build the LUT database. The simulated spectral bands correspond to the AISA spectral bands (particularly the spectral band no. 37, 38, 40 and 42; the wavelengths are indicated in table 2). The DART simulated spectral images were classified per each canopy closure into the following three thematic classes: illuminated tree crown (IC), shaded tree crown (SC) and non-covered ground. An average reflectance of shaded and sunlit crowns was extracted and a simple ratio between average reflectance of shaded and sunlit crowns were calculated and stored in the LUT’s for each combination of u_f and CC.

3.7. Methods of leaf area index retrieval

Two methods were applied for leaf area index retrieval from the remote sensing data of very high spatial resolution (the AISA image) using the LUT generated by means of the radiative transfer model DART. The selected inversion methods are: i) minimization of a cost function, and ii) application of the neural networks. The estimation of LAI was done for two extents of a sliding square window (dimensions of 10 and 8 meters), moving pixel by pixel over the AISA image. One u_f value and subsequently LAI value was extracted within the sliding window and assigned to the central pixel of the window.

3.7.1. Minimization of a cost function

The minimization algorithm was basically comparing simulated spectral LUT database values with observed AISA imagery hemispherical directional reflectance factor (HDRF) values and searching for the best matching case by means of minimizing a cost function (equation 11) in a LUT of corresponding canopy closure. Consequently, the

input leaf volume density (u_f) of the lowest RMSE was selected as an appropriate solution. The whole inversion procedure of the spectral LUTs was programmed and automated in Matlab environment by Raul Zurita.

$$RMSE = \sqrt{\frac{1}{n}\sum_{i=1}^{m}\left(R_{i,AISA} - R_{i,LUT}\right)^2} \quad (11)$$

First, the category of canopy closure was derived for the extent of a sliding window by means of calculating a ratio between number of crown pixels and the total number of pixels in the window. After that the ratio between shaded and sunlit crown pixels was calculated. The minimization algorithm was applied in proper canopy closure spectral LUT database calculating root mean square error (RMSE) between spectral values of the sliding window and LUT. The value of u_f for the case with the smallest RMSE was assigned to the central pixel of the sliding window. Afterwards the retrieved u_f values were converted into the LAI values using the canopy volume of the DART basic scenes.

3.7.2. Artificial neural networks

Neural network (NN) is a non-linear mathematical tool designed to estimate an unknown parameter based on the set of known input data. The most important part is to select the proper NN architecture and learn (train) properly your neural network for a desired response. A training dataset has to be build for learning purpose. The training set consists of the input data and known outputs. After the learning procedure, the neural network is applied to a testing dataset to derive the desired output values.

The look-up tables created from the DART simulations (section 3.6) were used as a training datasets. In total six training datasets were used, one for each canopy closure category. Chosen neural network belongs between the classification networks, which means that it is able to work only with the number in the range from 0 to 1. Thus all the values of leaf volume density (u_f) had to be normalized to fit the range.

There are many NN architectures available in the used software package ThinksPro. Unfortunately, there is no general rule to choose the best NN architecture. After testing several NN architectures the best performances were obtained for the Cascade architecture with the standard input setting, 10 nodes in one hidden layer and the quick propagation learning rule specified for hidden and output layer. The number of NN iterations was trained specifically per each canopy closure and it varied between 230 and 400 iterations. The testing dataset was created from the AISA image during the process of the cost function minimization (see section 3.7.1). The canopy closure value and the ratio between shaded and sunlit crowns reflectance for each spectral band were calculated within specific sliding window and assigned in to the central pixel. The NN architectures of each canopy closure were applied to the training spectral dataset to derive leaf volume density. The masks of the canopy closure categories of the sliding windows were used to filter the corresponding u_f values, which were afterwards converted into the LAI map of the AISA image subset.

4. Results

4.1. Field measurements of leaf area index

4.1.1. PCA-2000 measurements of LAI

The ground truth measurements done by PCA-2000 were post processed by the specialist from the ASCR providing values of the effective leaf area index per each point of the middle transect. The values of effective LAI had to be converted to the "true" LAI values. The revision of the conversion factor led to the similar value as published by Pokorny (2002). The value of 1.62 was used to obtain the "true" leaf area index values, applying a linear equation: $LAI = 1.62*LAI_{ef}$. The LAI values of transect points were ranging between 4.13 – 7.29 for LAI_{ef} and between 6.68 – 11.81 for LAI. The overview of the PCA-2000 measurement results is given in table 3.

Table 3. The values of effective leaf area index and the real values of LAI for each of the measured transect point.

point	LAI_{eff} 1	LAI_{eff} 2	average LAI_{eff}	true LAI
1	4.87	4.91	4.89	7.92
2	5.19	5.13	5.16	8.36
3	5.05	5.01	5.03	8.15
4	6.37	5.95	6.16	9.98
5	5.63	5.65	5.64	9.14
6	5	4.92	4.96	8.04
7	7.25	7.33	7.29	11.81
8	6.78	6.83	6.81	11.02
9	5.68	5.43	5.56	9.00
10	4.46	4.52	4.49	7.27
11	4.47	4.45	4.46	7.23
12	6.56	6.66	6.61	10.71
13	5.51	5.53	5.52	8.94
14	4.06	4.19	4.13	6.68
average	**5.49**	**5.47**	**5.48**	**8.87**

4.1.2. Hemispherical photographs and results from the CAN-EYE software

Hemispherical photographs processed by means of the CAN-EYE software provide estimates of both effective and "true" LAI (table 4). The average values of LAI were 2.82 and 4.88 for effective and "true" LAI respectively. The LAI values obtained from CAN-EYE were compared with the LAI estimates obtained from PCA-2000, see figure 9. The resulting LAI values from CAN-EYE are generally much lower than from PCA-2000. Destructive measurement of leaf area index within the same forest stand done in 1997 (Pokorny, 2002) indicated stand LAI around 8.5. Based on the comparison with destructive LAI measurement and with the PCA-2000 measurements the estimates of LAI by means of hemispherical photographs and CAN-EYE software were considered to be underestimated. Therefore, it was decided to exclude the results obtained from

hemispherical photographs from further analysis and validation of the LAI estimation from the AISA image.

Table 4. Summary of the effective and "true" LAI values obtained from the processing of hemispherical photographs using the CAN-EYE software.

plot	LAI_{ef}	true LAI
1	3.4	5.8
2	3.3	5.3
3	2.4	4.1
4	2.8	5.6
5	3	5.8
6	2.5	4
7	2.7	4.7
8	2.9	5.1
9	2.8	4.6
10	2.9	5
11	2.6	4.3
12	2.5	4.2
average	**2.82**	**4.88**

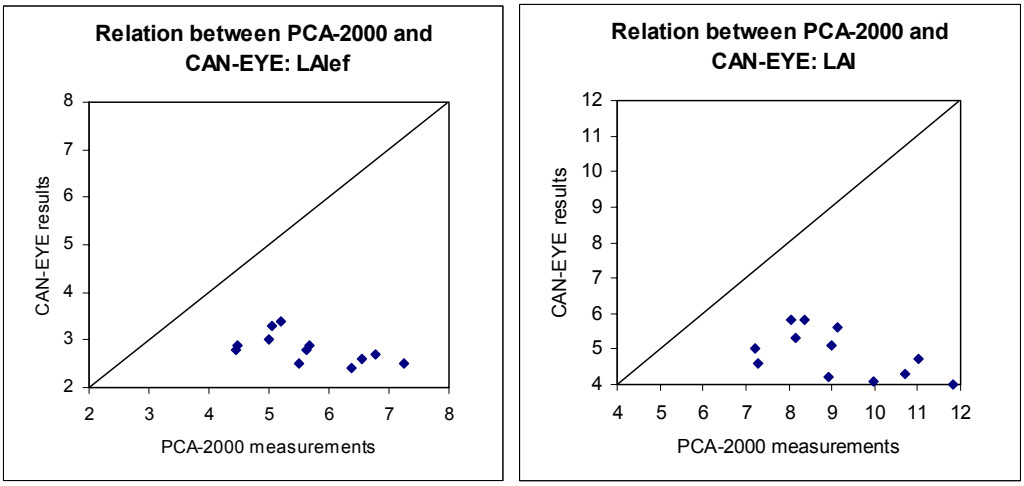

Figure 9. Comparison between PCA-2000 and hemispherical photographs estimates of effective LAI (left graph) and "true" LAI (right graph).

4.2. Results of DART parameterization and simulations

Proper parameterization of DART model was a very intensive and time consuming procedure, but it was the most essential step of the selected physically based study approach. Especially parameterization of newly introduced DART structural features (as described in sections 2.1 and 3.5.5) took a lot of time and raised many unexpected problems. This study demonstrates that it is feasible to obtain all the required input parameters for the case of a young Norway spruce forest stand. The most important intermediate results, obtained during the process of the DART parameterization, are summarized in the following paragraphs.

4.2.1. Structural characteristics of trees

The forest basic scenes in DART were build from four representative tees, trying to resemble the current growing stage of the young forest stand at Bílý Kříž study site. The overview of the simulated tree species basic allometric characteristics is given in table 5.

Coniferous trees, such as Norway spruce, are characterized by a highly organized structure of leaves within a crown. This kind of structural heterogeneity is introduced in DART through vertical and horizontal weights of leaf volume density u_f (described in chapter 3.5.5).

Vertical weights of leaf volume density were derived from the distribution of total leaf area in vertical direction for an average, suppressed and dominant tree. The graphs of vertical distribution (figure 10) indicate that most of the leaf area is cumulated between 20 -50 % of a tree height in case of an average tree, around 40% of relative height for a suppressed tree and between 25-60% in case of dominantly growing tree. The vertical weights reflected varying distribution of foliage in vertical direction, which is mainly affected by mutual position of trees within a canopy.

Digital reconstruction of the representative mature branches and their analysis in horizontal direction led to the expected horizontal distribution of leaf area as required for the DART simulations (compare figure 7 and figure 11). Two structural parameters (**β** and **γ**) were estimated as the results of the analyses of the leaf horizontal distribution. For the juvenile branches, which are related to the upper part of the "DART" trees, the **β** value was computed to be equal to 0.39 and **γ** parameter equal to 0.64. First productive branches, providing the estimates of the parameters for lower part of trees specified in DART, gave values of **β** and **γ** of 0.29 and 0.62, respectively (see figure 12).

The last parameter derived from the analyses of leaf horizontal distribution was the inner zone of defoliation indicated by parameter **a** (see section 3.5.5). The bottom radius of defoliated cone inside the crown, corresponding with the length of defoliated part of first productive branches, was found to be 23.3% of the average branch length.

Table 5. Basic allometric parameters of the universal trees used for DART simulations.

	Trunk height [m]		**Trunk diameter [m]**		**Crown radius [m]**		**Crown height [m]**
	below crown	inside of crown	below crown	inside of crown	bottom	upper	
Species 0	0.4	8.2	0.4	0.18	1.56	0.00	10.2
Species 1	0.2	7.0	0.2	0.15	1.26	0.00	9.0
Species 2	0.4	8.0	0.4	0.17	1.46	0.00	10.0
Species 3	0.6	9.2	0.6	0.20	1.83	0.00	11.2

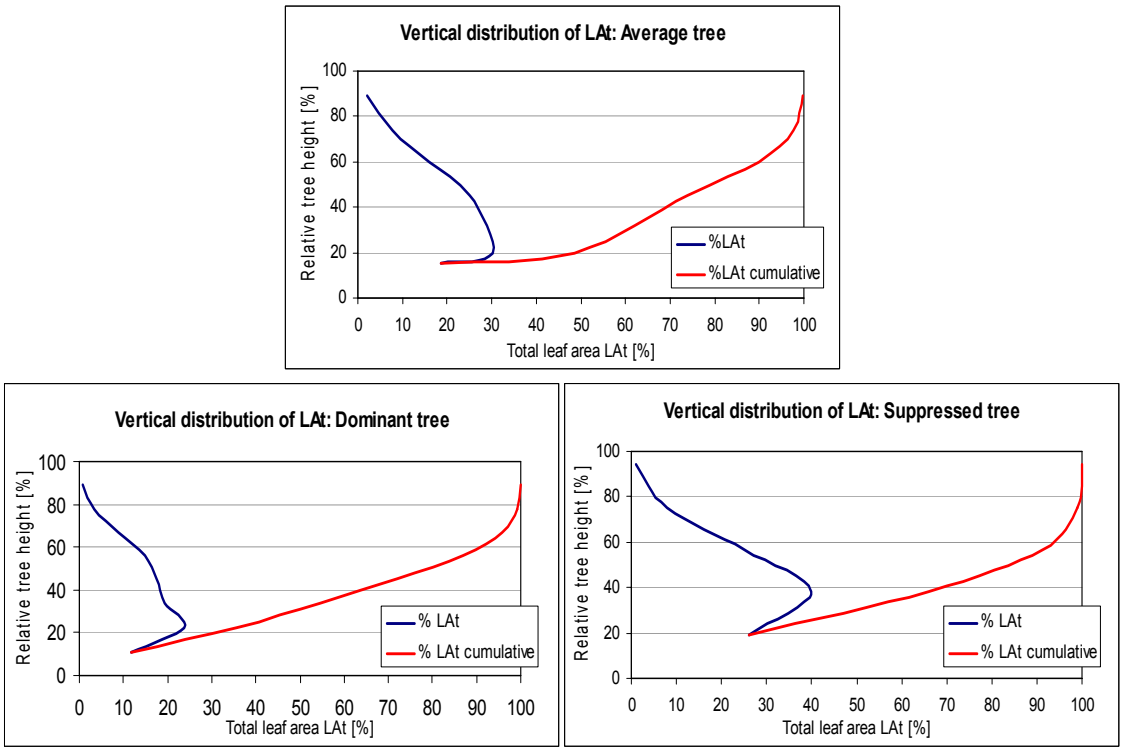

Figure 10. Vertical distribution of total leaf area [%] for an average, suppressed and dominant tree of the young Norway spruce forest stand.

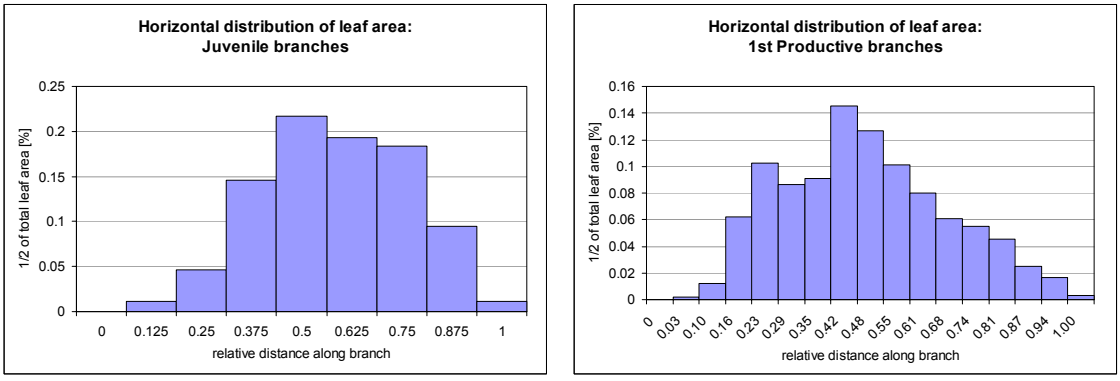

Figure 11. Horizontal distribution of leaf area based on the analysis of juvenile and 1st productive branches of mature spruce trees (Sumava Mts. 2003).

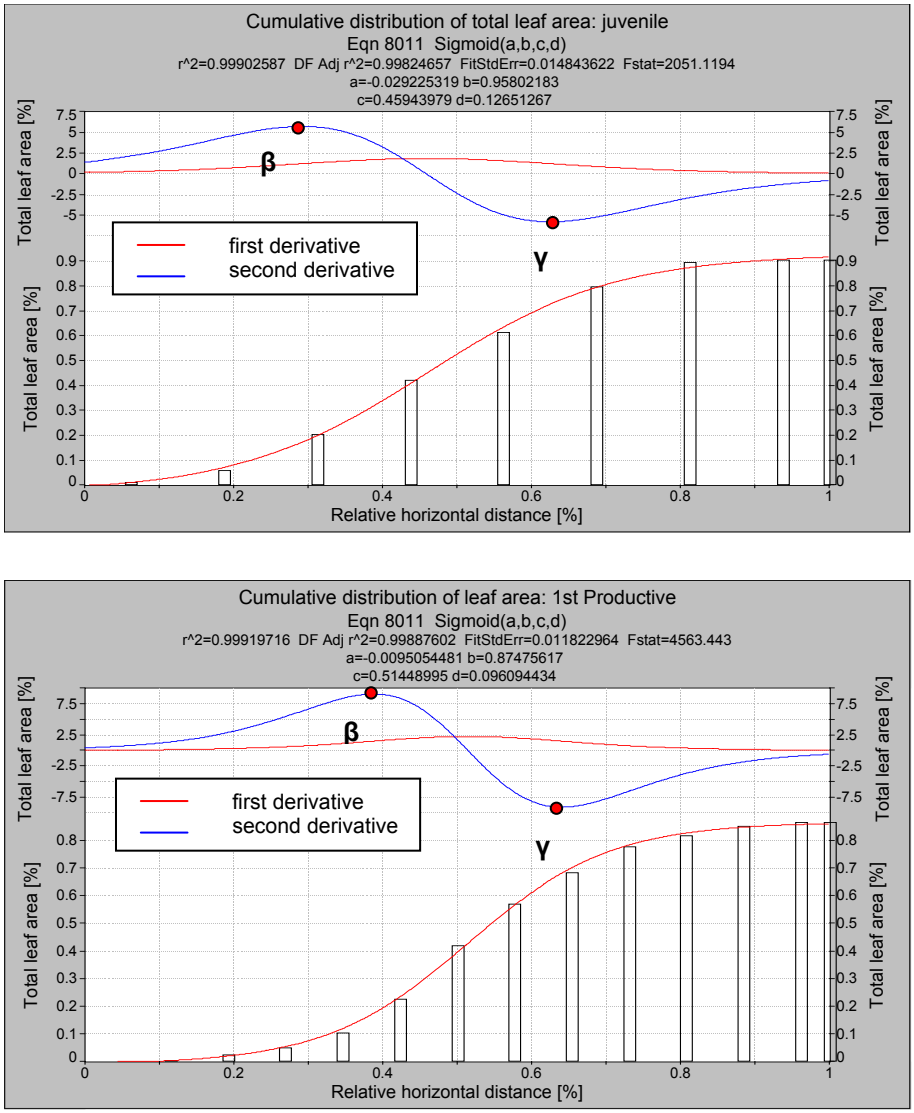

Figure 12. Determination of structural horizontal parameters (β and γ) of leaf volume density based on the analyses of representative branches (juvenile and 1st productive) of mature Norway spruce trees. Graphs were created by the trial version of TableCurve sowtware 2D version 5.01 (Systat **http://www.systat.com/**)

4.2.2. Optical properties of the DART scenes

Based on the measured optical properties of Norway spruce needles of last three age classes (see figure 13) and the distribution of needle age classes in vertical direction (table 6), the average optical properties (directional hemispherical reflectance and transmittance) of needles, used as a DART input, were calculated for seven vertical tree zones (see figure 14).

Extensive directional RT simulations in DART and their comparison with AISA image was conducted by Emmanuel Martin (CESBIO, France). This simulations stressed out that reflectance of the Norway spruce crowns, particularly in NIR part of spectra, is lower than observed reflectance values at AISA image (Martin, 2005). This fact led to the revision of input leaf optical properties. Values of transmittance in NIR were

compared with measured transmittance of Norway spruce needles from previous years, which indicated that optical properties used for DART simulations had in average 8% lower transmittance in NIR bands. Therefore, new optical properties were generated by means of linear increase of the transmittance intensity within the simulated NIR wavelengths (see table 2).

Table 6. Vertical distribution of needle age classes in percentage for the young Norway spruce trees obtained from destructive measurements (according to (Pokorny, 2002)).

	Relative tree height [%]	% of needle year classes			Needle type
		c	c+1	c+2 (r)	
I	0 – 15	1	5	94	shaded
II	15 - 30	11	15	74	shaded
III	30 - 45	25	51	54	shaded
IV	45 - 60	50	24.5	25.5	shaded + insolated
V	60 - 75	56.5	20.5	23	shaded + insolated
VI	75 - 90	63.5	25	11.5	insolated
VII	90 - 100	75	16	9	insolated

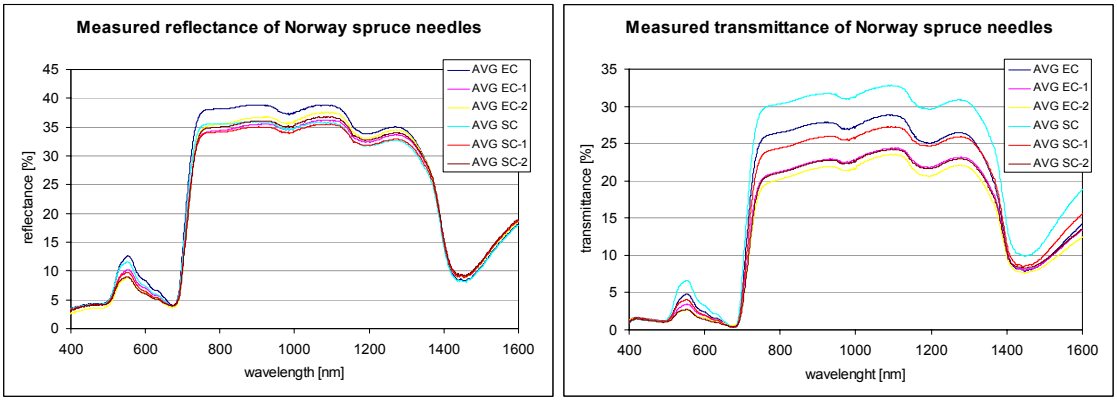

Figure 13. Measured directional hemispherical reflectance and transmittance by the field spectrometer (FieldSpec Pro) for the last three needle age classes (c, c+1 and c+2) of sunlit (EC) and shaded (SC) Norway spruce needles.

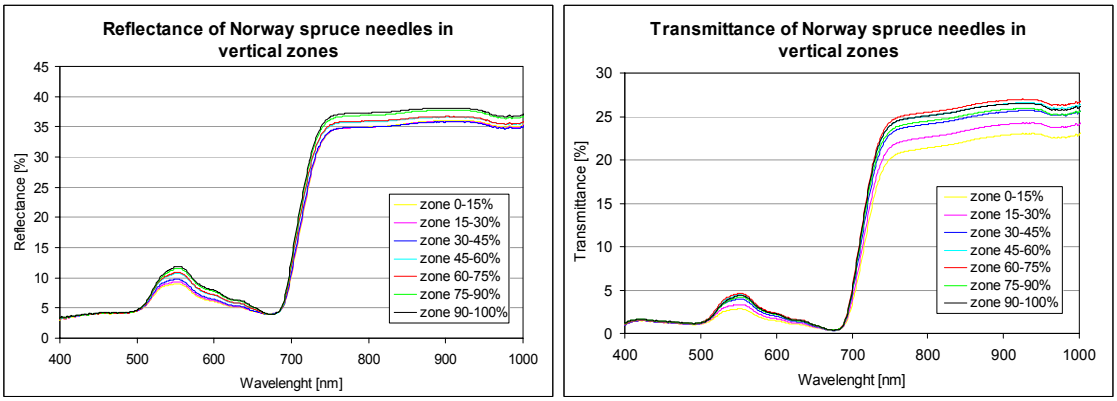

Figure 14. Final optical properties of Norway spruce needles in seven crown vertical zones, used as inputs of DART simulations.

Average optical property (reflectance) of ground cover used in DART is indicated in figure 15. The average reflectance at NIR plateau is around 25%. Calculated standard deviation of reflectance for the simulated spectral bands equal to 0.17 was used to introduce heterogeneity of the ground cover optical properties in the DART simulations. The optical properties of Norway spruce bark for trunks and branches are presented at figure 16.

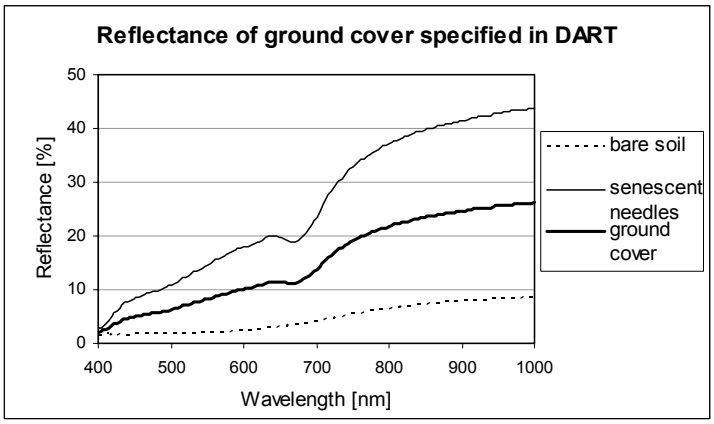

Figure 15. Reflectance of bare soil and senescent needles of the forest litter and the final optical property of the ground cover in the young forest stand, used as the DART input.

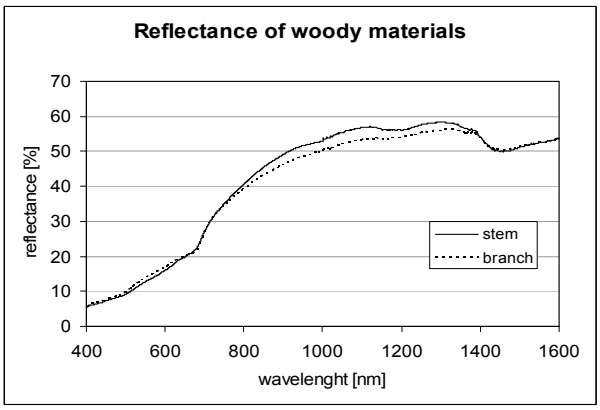

Figure 16. Optical properties (reflectance) of the Norway spruce branch and stem bark, used as the DART input.

4.2.3. Results of the DART simulations

A set of images for each spectral band was created for each simulated combination of canopy closure and leaf volume density. Example of NADIR view and one of the oblique views is given in figure 17. Shaded and sunlit crowns and shaded and sunlit ground cover could be easily detected at the images by visual as well as automatic classification. The average reflectance of the shaded and sunlit crown parts was extracted for each combination of u_f and CC and for each of the simulated spectral band (table 2). The example of the overall scene reflectance (BRF) and the average reflectance of shaded and sunlit crowns for the spectral band no. 42 are presented at figure 18. The spectral signatures derived for the rest of the simulated spectral bands can be found in appendix 2.

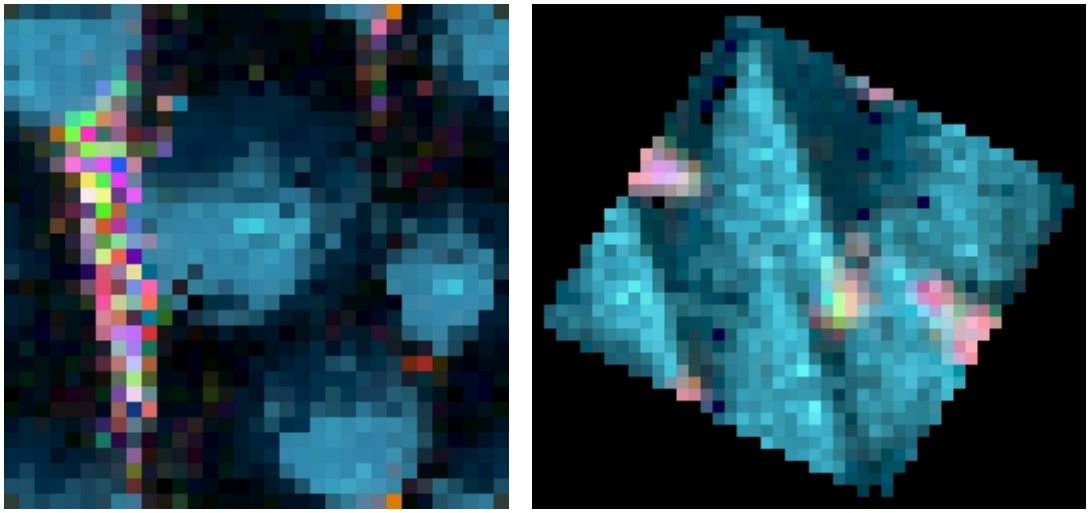

Figure 17. Example of the DART image outputs: representation of 55% canopy closure scene with u_f = 10 m^2/m^3; NADIR view (left) and oblique view (right). Both images are RGB colour composite (R 774, B 680, G 736 nm). The indigo blue represents the Norway spruce crowns and the pink colours represent the ground cover.

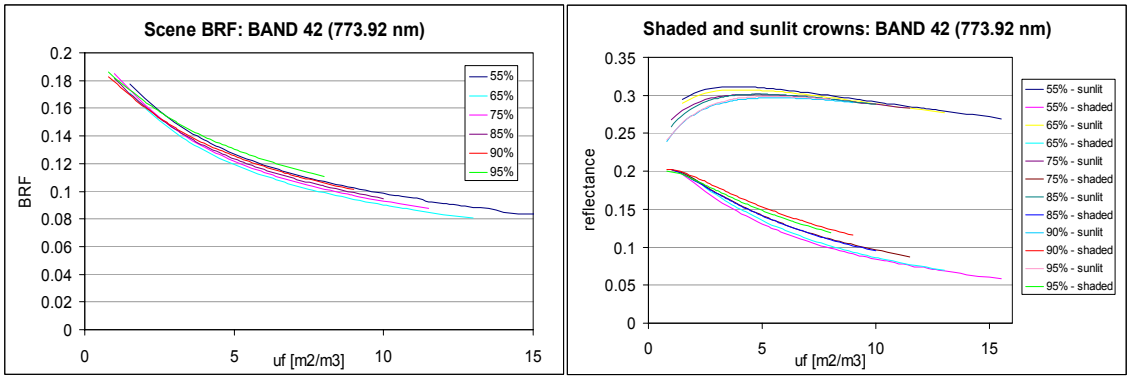

Figure 18. The spectral characteristics derived from the output DART images for each canopy closure category. The examples are given for the simulated AISA band no. 42. The average reflectance of the simulated scenes (BRF) is presented on the left graph. The average reflectance extracted from sunlit and shaded crown parts is presented on the right graph.

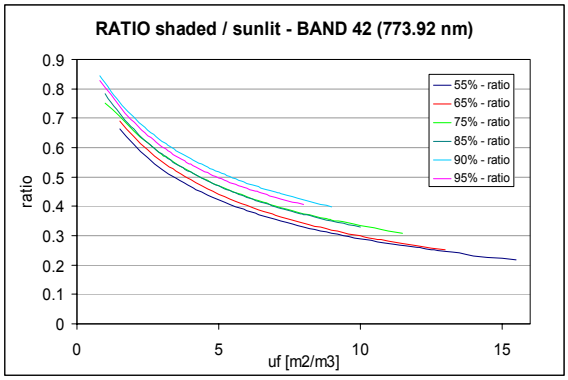

Figure 19. The spectral characteristic (the ratio between shaded and sunlit crown pixels) used to build the spectral LUT database. The example of the resultant ratios for each of the CC categories is presented for spectral band no. 42.

4.3. The look-up table database

The reflectance ratio between shaded and sunlit pixels of the Norway spruce crowns were calculated for each simulated combination of u_f and CC (the summary is given in appendix 1) and stored in spectral look-up table database. In total six LUTs were generated, each for one canopy closure category (section 3.5.4). The example of the ratio functions derived for the spectral band no. 42 is given at figure 19. The ratios for the rest of the simulated spectral bands are presented in appendix 3.

4.4. Processing of the AISA hyperspectral image

Example of the georeferenced AISA image lines after radiometric and atmospheric correction is given at figure 21. The ground measurements of reflectance of several ground cover surfaces, which were measured by the field spectrometer FieldSpec Pro during the flight campaign, were used to evaluate quality of the atmospheric and radiometric corrections of the AISA image. Comparing the measured ground reflectance and reflectance derived from the corrected AISA image for the same natural surfaces indicates good correlations within most of the wavelengths except several NIR spectral bands (from approximately 800 to 1000 nm), see figure 20.

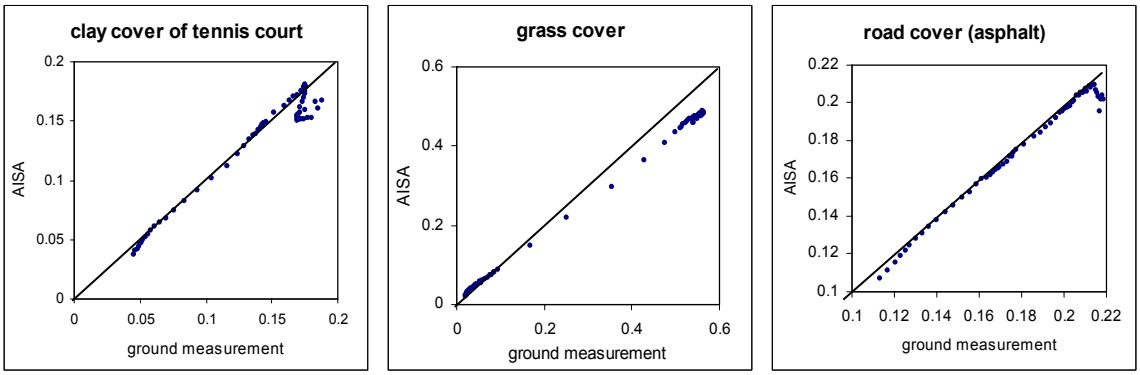

Figure 20. Evaluation of atmospheric and radiometric corrections of the AISA image. Comparison between ground measured and AISA derived reflectance of three selected ground cover surfaces.

Two different classification approaches, as described in chapter 3.4.4, were applied to the selected subset of the AISA image in order to properly differentiate shaded, sunlit Norway spruce crowns from the rest of the ground surface. The performances of both classification methods were evaluated by means of error matrixes using the testing regions of interest.

The overall accuracy of SAM classification was equal to 80.5%. The major problem of the SAM classification was the mixing of shaded and sunlit crown pixels. That is why Maximum likelihood classification approach was tested. MLH classification results in overall accuracy of 96%, improving significantly the separation of shaded and sunlit Norway spruce crowns. Because of that the MLH classification results were used further on in the LAI retrieval procedure. The error matrix for the MLH classification and

the result of classification are available in table 7 and figure 22. Producer and user accuracies of the MLH classification are given in table 8.

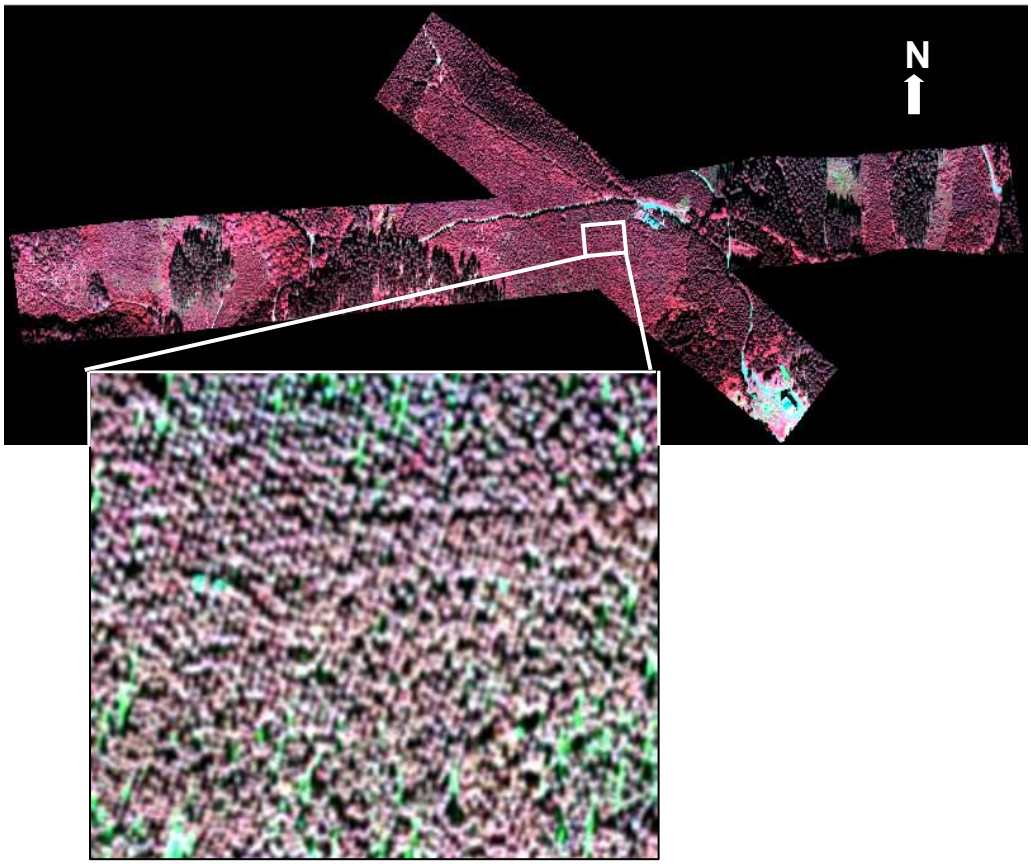

Figure 21. Example of the georectified mosaic of two AISA image flight lines of the spatial resolution of 0.4m and the AISA subset of the selected area of interest within the observed young forest stand.

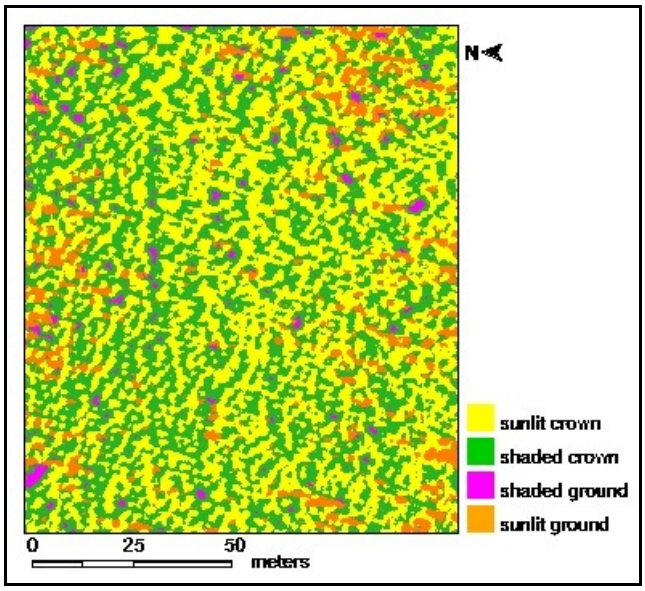

Figure 22. Classification result of the AISA image subset, using the Maximum likelihood classification.

Table 7. The error matrix for the MLH classification of the AISA image subset (the values are in percentage)

class name	testing data				
	shaded ground	illuminated crown	shaded crown	illuminated ground	**total**
shaded ground	91.82	0.00	0.00	0.00	15.23
illuminated crown	0.00	100.00	1.54	0.00	32.43
shaded crown	7.27	0.00	92.31	0.00	28.36
illuminated ground	0.91	0.00	6.15	100.00	23.98
total	100.00	100.00	100.00	100.00	100.00

Table 8. Overview of producer and user accuracies, overall accuracy of the MLH classification and kappa coefficient.

class name	Producer accuracy [%]	User accuracy [%]
shaded ground	91.82	100.00
illuminated crown	100.00	98.60
shaded crown	92.31	95.74
illuminated ground	100.00	95.74
overall accuracy	**96.38**	
kappa coefficient	**0.957**	

4.5. Results of leaf area index estimations from the AISA image

Two methods retrieving the leaf area index form AISA image subset were used and evaluated within this study: i) minimization of a cost function, and ii) application of neural networks. These methods of LAI retrieval were not a pixel based, but the sliding windows of two extents (10 m and 8 m), moving over the AISA image, were applied. Application of LAI retrieving methods resulted in spatial maps of leaf volume density u_f and subsequently maps of leaf area index distributions over the observed forest stand. The values of LAI were not retrieved directly, but first leaf volume density u_f was estimated for each sliding window position. After that u_f was recalculated into the LAI using a simple linear relation (equation 12) with conversion coefficients (see table 9) based on the canopy volume.

$$LAI = c * u_f \quad (12)$$

The canopy volume was directly derived from the DART scenes of each canopy closure, as shown in figure 23. The volume of canopy was systematically decreasing with increasing canopy closure. Only in case of 90% CC the canopy volume was out of

expected range, which might be due to the number rounding in DART. Therefore, the canopy volume of 90% CC was adjusted to fit a linear decreasing trend and corresponding conversion coefficients table 9 was calculated from the adjusted value.

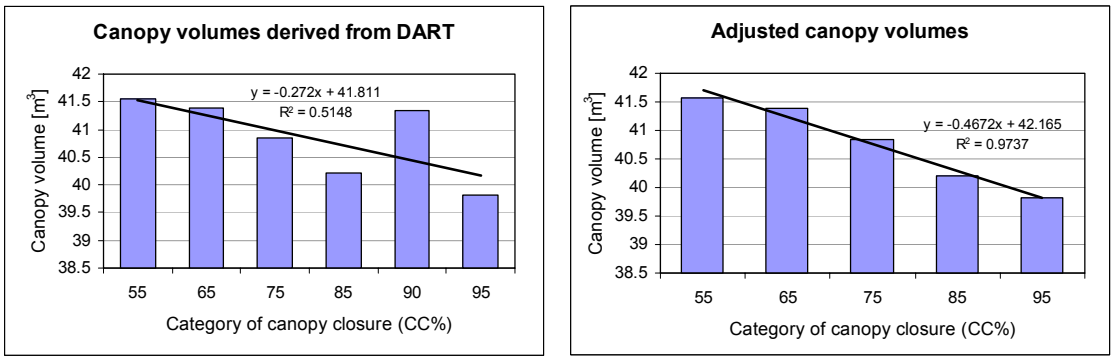

Figure 23. Canopy volumes for each CC representation derived directly in DART (left) and linear regression for canopy volume correction of outlying 90% CC (right)

Table 9. Canopy closure coefficients for conversion of retrieved leaf volume density into the LAI values

Canopy closure [%]	conversion coefficients
95	1.8817
90	1.6066
85	1.4983
75	1.3030
65	1.1448
55	0.9541

4.5.1. Canopy closure of the forest stand

Application of the sliding windows over the MLH classification of the AISA image produced spatial outputs of canopy closure categories (figure 24). This additional information was needed to convert spatial maps of u_f, resulting from the minimization method and the neural network approach, into the map of LAI distribution.

The mean canopy closure of the young forest stand was equal to 89% with standard deviation of 8.33% for 10m sliding window. In case of 8m sliding window the average canopy closure was 88.6% with standard deviation of 9.08%. In both cases 95% CC class was the most abundant, particularly 49.02% of whole forest stand area in case of 10m sliding window and 49.91% and for the sliding window of 8m.

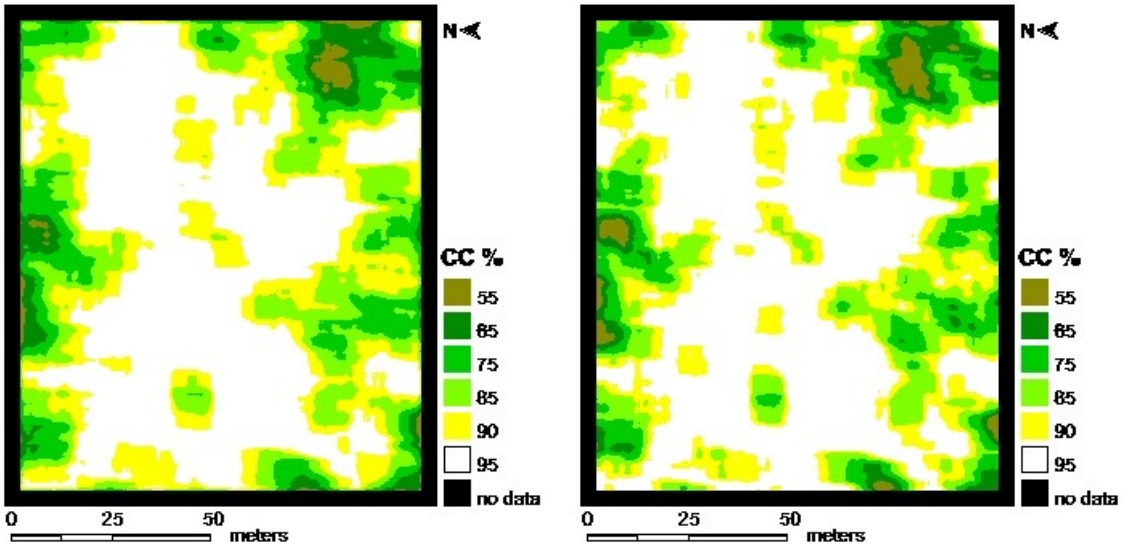

Figure 24. Map of canopy closure categories generated form the MLH classification of the AISA image for the sliding window of 10m (left) and 8 m (right) in size.

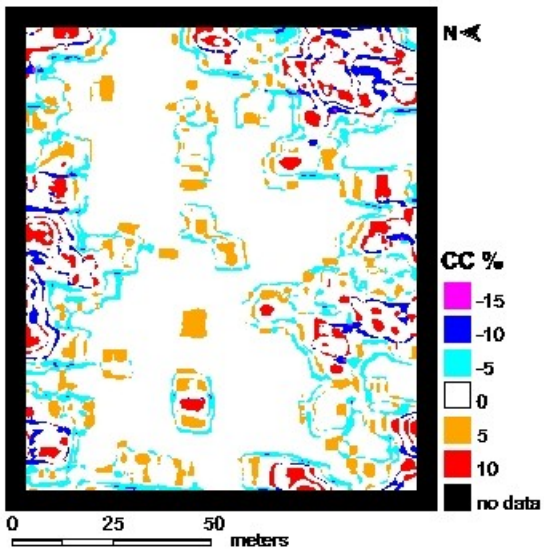

Figure 25. The spatial map of the differences between canopy closures derived for two sliding window extents (the result of subtraction: win 10m – win 8m)

4.5.2. Minimization of a cost function

The results of the spectral LUT inversion by means of a minimization cost function per each extent of sliding window are given in figure 26 for leaf volume density, and in figure 27 for forest canopy leaf area index. The mean u_f values of the observed forest stand were 3.748 m^2/m^3 and 3.733 m^2/m^3 for the sliding window of 10 m and 8 m respectively. The average value of the estimated forest stand LAI was 6.35 for 10 m sliding window and 6.307 for 8 m sliding window.

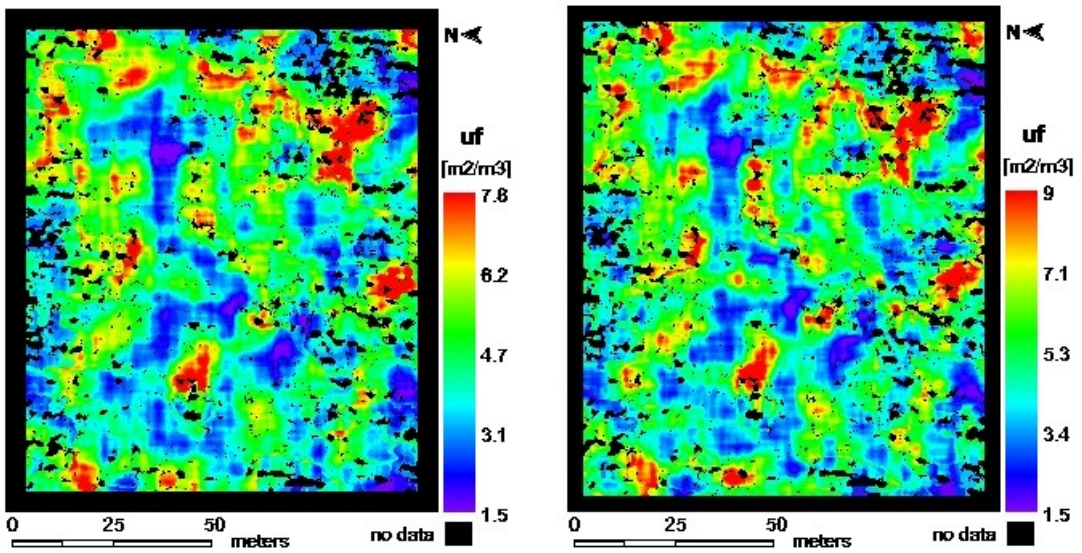

Figure 26. Minimization approach: maps of estimated leaf volume density u_f [m^2/m^3] from the AISA image for the sliding window extent of 10 m (left) and 8 m (right).

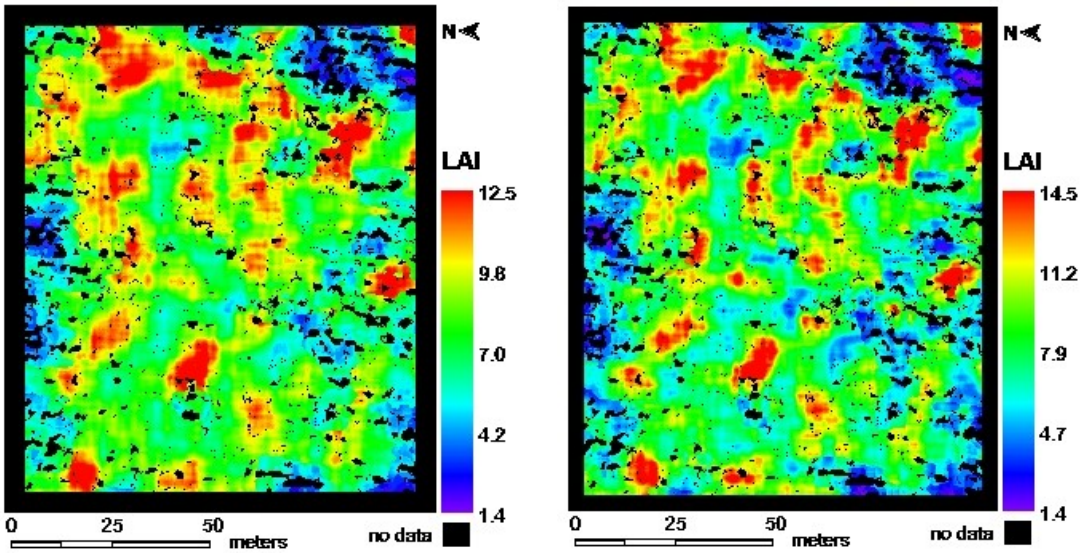

Figure 27. Minimization approach: maps of estimated leaf area index from the AISA image for the sliding window extent of 10 m (left) and 8 m (right).

4.5.3. Artificial neural networks

The results of the spectral LUT inversion by means of the neural network approach, including both sliding window extents, are given in figure 28 for leaf volume density, and at figure 29 for leaf area index. The mean retrieved u_f values of the observed forest stand were equal to 3.667 m^2/m^3 and 3.687 m^2/m^3 for the sliding window of 10 m and 8 m respectively. The average estimated LAI of the observed forest stand was 6.197 for 10 m and 6.141 for 8 m sliding window.

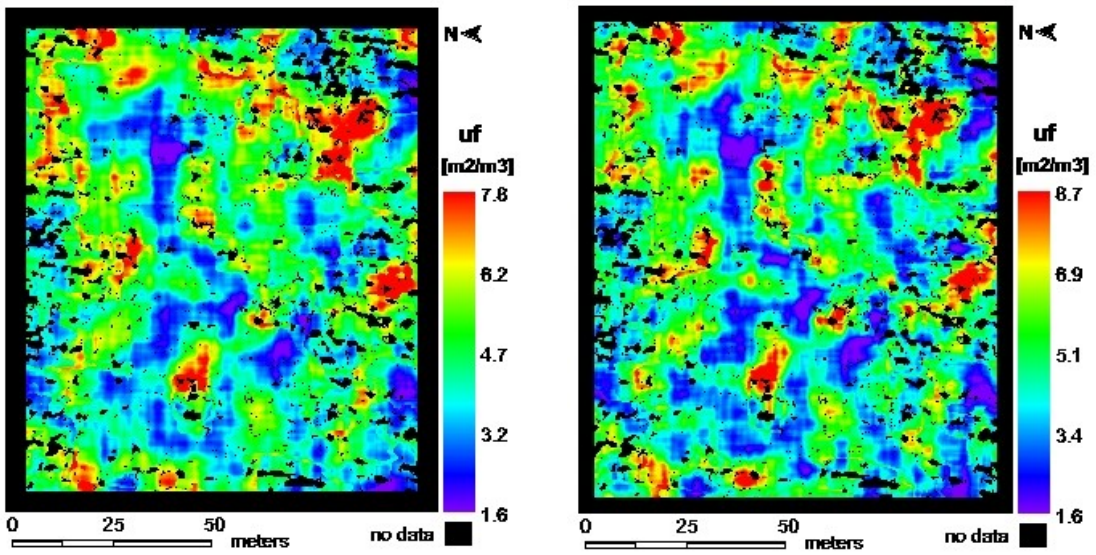

Figure 28. Neural networks approach: maps of estimated leaf volume density u_f [m^2/m^3] from the AISA image for the sliding window extent of 10 m (left) and 8 m (right).

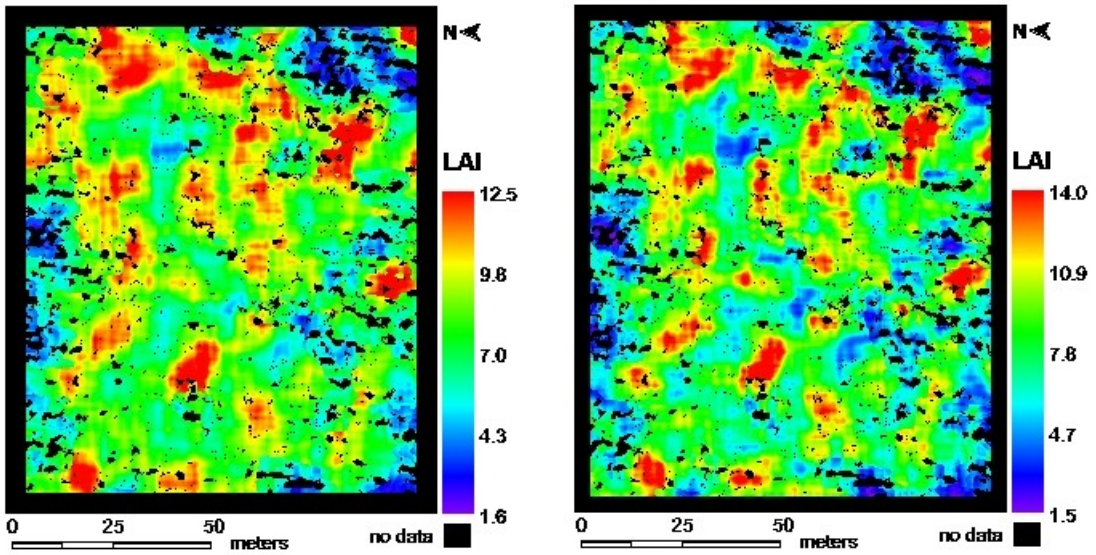

Figure 29. Neural networks approach: maps of estimated leaf area index from the AISA image for the sliding window extent of 10 m (left) and 8 m (right).

4.5.4. Evaluation of the LAI retrieving approaches

The short summary of the estimated LAI and u_f values for the whole observed forest stand is presented in table 10. The field measurements of leaf area index obtained form the Li-Cor PCA-2000 were used for the validation of the LAI values estimated from the AISA image subset. One-to-one relations between ground measured and hyperspectral image retrieved LAI values are indicated in figure 30. In addition, the predicting capability of each inversion method was evaluated within the root mean square errors (RMSE) and Pearson correlation coefficients, which are shown in table 11.

Table 10. The summary of the estimated LAI and u_f values from the AISA image by means of neural network inversion approach and inversion by minimization of a cost function for each extent of the sliding window (10 and 8 meters). The values are extracted from the spatial maps of LAI and u_f , presented at figures 26 – 29.

		Cost function		Neural Networks	
		win10	**win 8**	**win10**	**win 8**
uf [m2/m3]	**mean**	3.748	3.733	3.667	3.687
	st. dev.	0.721	0.860	0.718	0.855
	min	2.000	1.500	1.841	1.591
	max	7.800	9.000	7.780	8.688
LAI	**mean**	6.350	6.307	6.197	6.141
	st. dev.	1.414	1.640	1.337	1.564
	min	2.290	1.431	2.332	1.681
	max	12.531	14.460	12.499	13.959

Table 11. Overview of the LAI retrieving methods performances by comparison with the field measurements of LAI (PCA-2000).

Method	**mean**	**R***	**Sig.****	**RMSE**
Minimization cost function (window 10m)	7.12	0.024	0.936	2.457
Minimization cost function (window 8m)	7.07	0.094	0.748	2.427
Neural Networks (window 10m)	6.88	0.080	0.979	2.629
Neural Networks (window 8m)	6.84	0.064	0.828	2.613

* Pearson correlation coefficient; ** significance within confidence interval of 95%

Table 12. Pearson correlation coefficients (R) computed between used inversion methods (LUT min = inversion of the LUT by the minimization cost function; NN = inversion of the LUT by the neural networks).

pair of method	**R**	**sig.***
LUT min (win 10m) x LUT min (win 8m)	0.985	0.000
NN (win 10m) x NN (win 8m)	0.984	0.000
LUT min (win 10m) x NN (win 10m)	0.998	0.000
LUT min (win 8m) x NN (win 8m)	0.999	0.000

- significance within the confidence interval of 95%

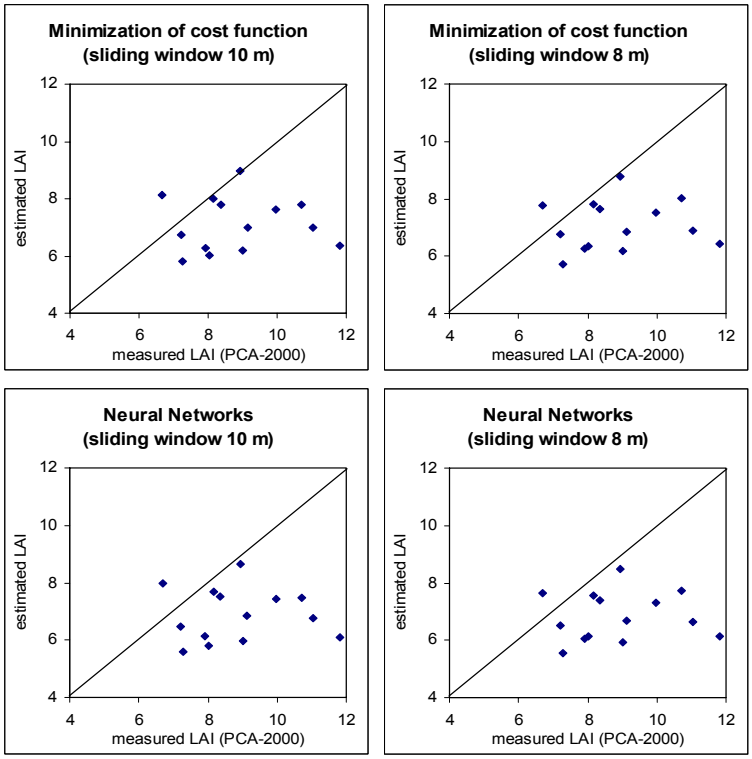

Figure 30. Comparison of the methods of LAI retrieval against the ground measurements; left graphs corresponds to sliding window extent of 10 m and right graphs to 8 m sliding window.

Subtraction the map of LAI estimated by the minimization cost function from the LAI map of the NN approach (see figure 31), the following mean difference values were obtained: -0.142 and -0.153 for the sliding window extent of 10m and 8m. These results showed that neural networks provide slightly lower estimates of LAI than minimization function approach.

The evaluation of the effect of different sliding window extent on the LAI estimation was done through subtraction of the final LAI map for window of 8m from window of 10m per each inversion method. The results of the subtraction are presented in figure 32. The mean values of resulting images are 0.026 and 0.012 for NN and minimization approach, respectively.

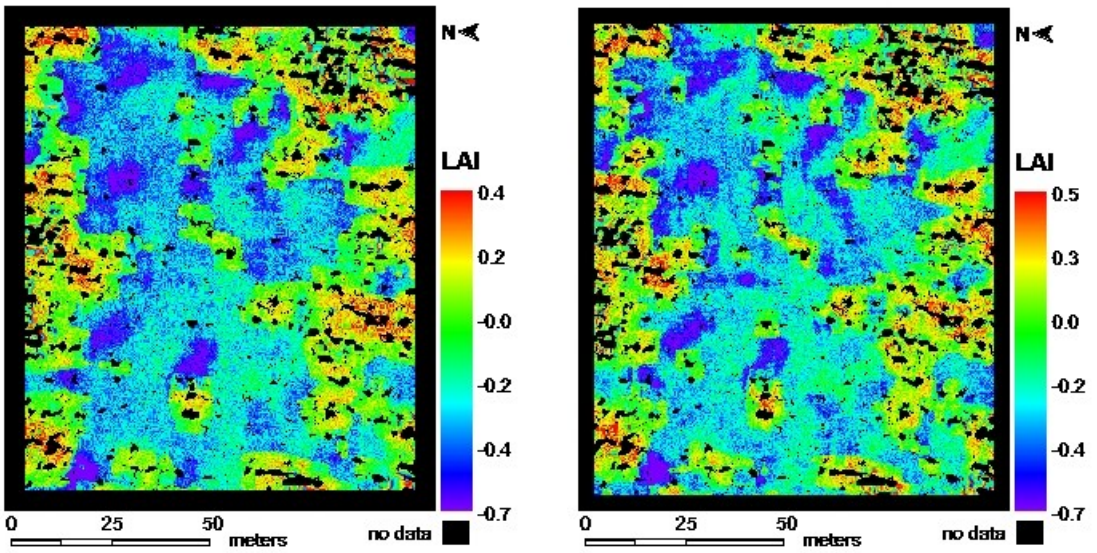

Figure 31. Spatial map of subtraction between both LAI retrieval methods (NN – LUTmin) for the window extent of 10m (left) and 8m (right).

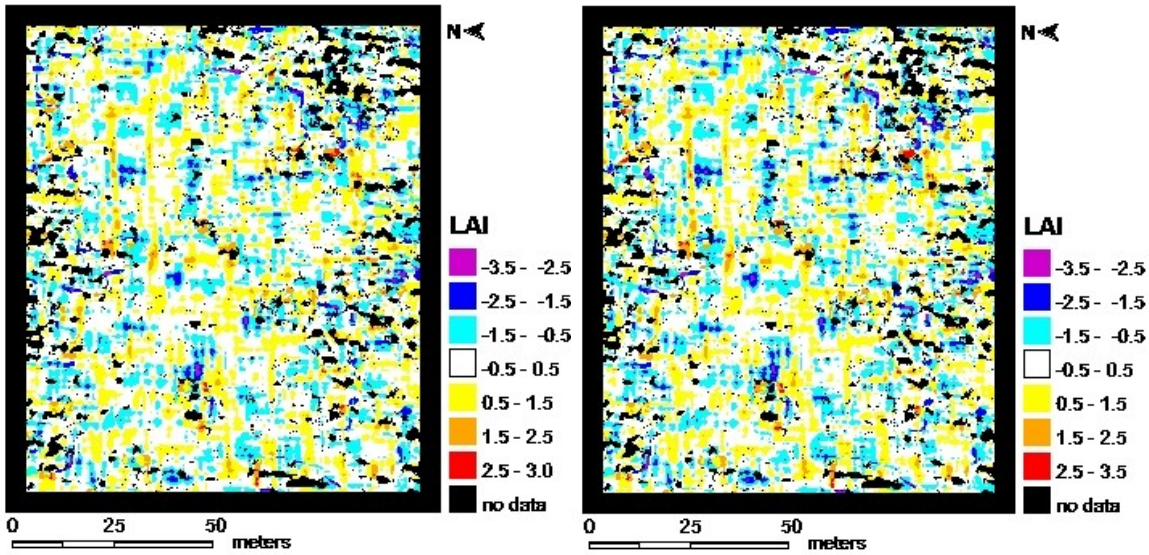

Figure 32. Spatial map of subtraction between two different extents of sliding window (win.10m-win.8m) for neural network approach (left) and minimization approach (right).

5. Discussion

5.1. Leaf area index obtained from field measurements

Ground truth data for the validation of LAI retrieved from the AISA image were collected by means of two indirect optical methods: i) plant canopy analyzer (PCA-2000), and ii) hemispherical photographs taken by a digital camera equipped by the fish-eye lens. Both devices are deriving effective leaf area index (or plant area index) from the gap fraction distribution. The measurements have to be free from the influence of woody materials and clumping effect of foliage elements to obtain true values of LAI. The coefficient to correct PCA-2000 measurements was presented by (Gower, Norman, 1991) as 1.6 for Norway spruce canopies. The coefficient is in agreement with the results of Pokorny (2002), derived for the 0-43º field of view of PCA-2000. Our revision of the correction factor led to the similar result (1.62), which suggests universality of the LAI_{ef} correction coefficient for young Norway spruce stands.

The original motivation why to acquire hemispherical photographs was a possibility to eliminate the effect of woody materials (branches and trunk) during the post-processing of the images in CAN-EYE software. The presence of woody parts is an important source of errors (Chen, Rich et al., 1997) when estimating LAI from gap fraction. Although, the processing of the hemispherical photographs in CAN-EYE allowed discrimination of wood from leaves, in the next processing step the class “wood” had to be assigned to either leaf or sky class. We chose to assign the wood class into the class of leaf, which should lead to the potential overestimation of LAI. Nevertheless, the results presented in section 4.1.2 showed lower estimates of “true” and effective LAI and poor correlation with PCA-2000 measurements.

The direct destructive measurement of leaf area index provided the LAI of 8.6 for the same young forest stand in 1997. The lower estimates by means of hemispherical photographs have been reported by Kraus (Kraus, Broich et al., 2005). He mentioned possible saturation of LAI_{ef} estimates around 4-5 for the method of LAI measurement using hemispherical photographs. This statement corresponded to our results. The mean values did not exceeded 3 and 5 for case of LAI_{ef} and LAI, respectively. Very high values of LAI, measured by PCA-2000, were not revealed from the hemispherical photographs.

One of the possible causes of LAI underestimations could be inappropriate sampling scheme. CAN-EYE software is mainly used for processing of hemispherical photographs acquired within a VALERI sampling plot (Baret, Weiss et al., 2005). Such a plot consists at least out of 12 sample points, over those a special neural network (NN) is created during the image processing. Our sampling scheme was a matrix of only 3x3 observation points, which might be insufficient number for NN architecture of CAN-EYE.

5.2. AISA image post-processing

The result of the MLH classification was used to derive the canopy closure over the AISA image subset and reflectance ratio of sunlit and shaded Norway spruce crowns. Both of the products were directly used during the retrieval of leaf area index from the AISA image, thus the accuracy of the retrieval results depends on the accuracy of the image classification.

The canopy closure was calculated as the ratio between number of crown-classified pixels and total number of pixels within a window extent. Unfortunately, the edges of the crowns appeared in shades of surrounding trees, which is represented by a low and noisy signal. It was very difficult to determine a clear boundary between the Norway spruce crowns and ground cover based purely on spectral information. The advantage of used AISA image was its very high spatial resolution (0.4 m pixel size) which allows detection of individual tree crowns even in a dense coniferous stand. Application of an automated detection and crown delineation (segmentation) algorithm (Gougeon, 1995; Culvenor, 2002; Leckie, Gougeon et al., 2005) could lead to more reliable results in calculation of canopy closure. When delineating crowns properly, the background could be masked, and the classification algorithm might be applied only on the detached crown pixels. This might improve the separation between the shaded and sunlit parts of the crowns.

5.3. DART parameterization

The proper parameterization of DART was the most time demanding step of the whole study. The new version of DART model, offering new forest structural parameters (see section 2.4), was used within this research. It was assumed that new features implemented in DART will improve the overall performances of RT simulation. It would be necessary to evaluate the effect of the new parameters by means of sensitivity analysis and comparison the performance with the old DART version, which is not objective of this study.

5.3.1. Structural characteristics of young Norway spruce trees

The DART representation of a tree is a geometric simplification of the reality. Taking the advantage of the new structural parameters (described in section 2.4 and 3.5.4), we tried to depict the real growing strategy and crown architecture of the young Norway spruce trees.

Basic allometric characteristics (table 5) of the “DART trees” were based on the extensive field measurements in 1997 (Pokorny, 2002), and recalculated to the current growing stage of the trees. It was necessary to adjust the original field data according to requirements of the DART model simulations. For instance, the height of the trunk within crown had to be shortened by two meters to minimize strong effect of trunk reflectance in the upper part of simulated canopy. The presence of a trunk, in combination with a very narrow conical shape at the top part of a crown, led to the unrealistic pattern, visible on the output images of simulated spectral bands.

Several geometric simplifications of a tree crown shape are available in the DART model. The truncated cone, with the upper diameter equal to zero, was applied in this study. Rautiainen (2004) studied the effect of four crown shapes (conical, ellipsoid, cylinder and cylinder+cone) on the reflectance of Norway spruce stand. For higher values of LAI, stands with conical crowns had much smaller reflectance than ellipsoid crowns. Further comparison of tree crown shapes showed the smallest scattering for cylindrical crowns, highest for the ellipsoid and combination cylinder+cone somewhere in between. Unfortunately, no comparison was made to the real images of coniferous stands to conclude which crown shape was the best fitting. The field observation of Norway spruce trees indicates that much better approximation of the crown shape should be a combination of truncated cone with cylinder at the top. It would be interesting to evaluate the best crown shape for Norway spruce using the DART model, and compare the results with real reflectance values of the airborne images (AISA). Especially to compare the current DART representation of a crown used for Norway spruce (truncated cone with zero top radius) with the proposed combination of truncated cone + cylinder.

The determination of the horizontal distribution of leaf volume density and distribution of empty cells was based on destructive analysis of the mature branches, because similar data were not available for a young forest stand. This age discrepancy might be a source of potential errors. The mature branches, especially the first productive branches, have more heterogeneous structure than young branches due to the general differences in the crown architecture. When analyzing the branches in horizontal manner we were assuming that the branches were not overlapping each other within a whorl. This assumption does not fully agree with the reality, because small parts of the neighboring branches within the whorl can overlap. Thus, it is not easy to determine a representative space occupied by a branch inside the crown collecting just a one sample branch (see figure 8). The growing strategy of a tree is to occupy the empty spaces evenly. It means that branches can substitute each other within a whorl or even from adjacent whorls if there is an empty space in the crown. It was impossible to describe this fact with our field data and thus the results concerning the horizontal distribution of the leaf area within the crown may not represent the real distribution properly.

Light Detection and Ranging (LiDAR) devices are widely used in forestry to depict horizontal and vertical structure of a forest stand. LiDARs have been used to detect canopy (Zimble, Evans et al., 2003) or individual tree (Persson, Holmgren et al., 2002) height. Roberts et. al. (2005) estimated a leaf area of individual loblolly pines. The LiDAR technique might be more appropriate solution to describe vertical and horizontal structure of foliage elements and overcome the drawbacks of the field destructive methods.

5.3.2. Optical properties used for DART simulations

The input optical properties of scene elements can be either measured or simulated by a leaf reflectance model (Jacquemoud, Baret, 1990). Within this research, all the

optical properties used in DART (figures 13 – 16) were measured. The advantage of the new version of DART model is an option to specify different leaf optical properties in the vertical direction of tree crowns, which increase the inner heterogeneity of the crowns. Another way how to increase variability of optical characteristics is by specifying a standard deviation value. Unfortunately, only one value can be defined for all the wavelengths. It would be more appropriate to specify this standard deviation separately for reflectance and transmittance and even more, specifically for each particular spectral wavelength.

The extensive directional RT simulations, carried out by Martin (Martin, 2005), indicated differences between DART simulated and AISA measured reflectance of the selected subplot of the Norway spruce stand. The simulated reflectance was lower than the observed one. The reason could be either wrong specification of the optical properties of Norway spruce needles (section 4.2.2) or inappropriate implementation of new DART structural features (section 2.4). Currently, we are not able to evaluate the effect of the new structural features, this should be done in near future. Therefore the revision of the optical properties was the only option to solve the underestimation problem. The Daughtry method (Daughtry, 1989), used to measure the optical properties of conifer needles, can underestimate the transmittance signatures due to a gap fraction between measured conifer needles. Mesarch et al. (1999) studied this effect and conclude that gap fraction less than 20% yields acceptable transmittance values. The gap fraction of our measured samples was in average 28%, which could result in underestimation of the needle transmittance signature. This conclusion is supported by the comparison with transmittance of Norway spruce needles measured in previous years, which reveals 8% decrease in transmittance of NIR part of spectra.

5.3.3. Results of RT simulations

In general a decrease of the simulated scene BRF with increasing leaf volume density was observed within the NIR spectral bands. The similar decreasing trend was observed for the average reflectance of shaded and/or sunlit crowns (as indicated in figure 18 and appendix 2). This might be explained in a following way. Increase in leaf volume density means higher amount of foliage which can absorb more radiation. This leads to lower scattering between the leaves and woody elements (branches and trunk), which finally decrease the NIR reflectance of simulated canopy. This relation, described as the exponential function, was used to estimate LAI from the AISA image.

The decrease of canopy volume, directly derived from the DART basic scenes (figure 23), was expected with increasing canopy closure. The number rounding within the DART model adjusts dimensions of the objects according to the scene size cell size (0.2m in our case). This rounding is responsible for slight changes in tree position, even if their exact coordinates were specified. Unfortunately, even a small shift in tree positions can affect significantly the final canopy closure and consequently the canopy volume, especially if the basic scene is rather small. Secondly, the accuracy of canopy volume calculation depends on the dimension of basic scene cell and on the percentage of empty/full leaf cells within a canopy. Hence, it would be more appropriate

to generate the real volume of the observed canopy directly from an additional measurements, e.g. from a LiDAR observation.

5.4. Results of the leaf area index retrieval

5.4.1. Ratio between shaded and sunlit crown pixels

First, the average reflectance (BRF) of the whole scene was extracted for each spectral band of each canopy closure category. The results are presented in figure 18 and appendix 2. The relation between leaf volume density and average scene BRF indicated the saturation for the high values of leaf volume density. The saturation leads to impossible identification a unique value of u_f for a particular scene reflectance, which is called ill-posed problem (Combal, Baret et al., 2003).

The very high spatial resolution of the AISA image (0.4 m) allowed us to differentiated individual tree crowns. Even further, shaded and sunlit part of Norway spruce crowns could be distinguished. Exclusion of the forest background and extraction of the reflectance only from the individual crowns increased the purity of the information content and reflect an actual state of the only forest canopy. The reflectance ratio between shaded and sunlit crown pixels did not indicate such a strong saturation for high u_f values as the scene BRF. That is why, the ratio was considered to be more suitable spectral parameter for the LAI retrieval.

5.4.2. Sliding window extent

The extent of the window, sliding over the AISA image during the LAI retrieval, was one of the factors determining the canopy closure category and the reflectance ratio between the shaded and sunlit crown pixels. The minimum extent of our sliding window was driven by the condition that both categories, shaded and sunlit crowns, had to be present within the window. We have used only two different window extents, but it would be appropriate to explore systematically what is the effect of the changing window dimensions and the optimum window size for the LAI retrieval.

5.4.3. Canopy closure

A priori knowledge about the canopy closure is used in this study to prevent so called ill-posed problem of the spectral LUT inversion (Combal, Baret et al., 2003), i.e. the possibility to find two or more LAI solutions for one spectral value stored in the LUT. The canopy closure category was directly derived from the classified AISA image using a sliding square window of varying size. The classified CC category, assigned into the central pixel of the sliding window, is influenced by the window dimensions. From figure 25 one can interpret that the most frequent difference between CC images for both extents of the sliding window is equal to zero, followed by difference +/- 5% and more. Hence we can conclude that used extents of the sliding window are not the major drivers of the uncertainty behind the canopy closure and subsequently LAI estimation from the AISA image.

5.4.4. Retrieval of LAI by means of minimization by a cost function and neural networks approach

According to RMSE values shown in table 11, the minimization approach inverting the spectral LUT for the sliding window of either 10 m or 8 m could be evaluated as slightly better performing method than neural network approach. However, low values of the Pearson correlation coefficient R, computed between ground measured and estimated LAI, suggest their very low dependency, and also low accuracy of the LAI estimation. As shown in figure 30 and figure 33, none of the retrieval methods was capable to estimate accurately high values of LAI (generally higher than 9 and 10). It seems that spectral ratio of the shaded and sunlit crown pixels is still not sufficient enough to distinguish the high leaf volume density of the crowns. The exponential function describing relationship between LUT reflectance signature ratios and leaf volume density is flattening for high values of u_f (see figure 19), which means that small change in AISA spectral information causes important change in retrieved LAI value. Integration of the spectral bands from red and/or SWIR part of the electromagnetic spectra may help to resolve this spectral saturation and improve the LAI estimation.

The difference between measured and average retrieved LAI bigger than 2.5 was established to find the outlying LAI values. Although the Pearson coefficients increased after exclusion of the outliers, they sill remained non-significant on the significance level of 0.01 (see table 13). An explanation of this LAI prediction bias is uncertainty in the ground measurements of leaf area index by PCA-2000. The measurements were carried out only for the middle transect of the sample points and the complete set of the measurements was repeated only twice. The sampling scheme of the transect points was set up in order to cover the variability of the young forest stand densities (the dense and sparse part of the forest). However, the visual interpretation of the ground measurements results did not reflect any clear difference between the dense and sparse part of the young forest stand. The revision of the sampling scheme and more ground measurements of LAI should increase the reliability of the PCA-2000 ground measurements.

Positioning of the transect ground measurement points within the AISA image subset might be another source of uncertainties. Shift in position of the ground points on AISA image causes inappropriate location of the PCA-2000 hemispherical FOV, which means that LAI values obtained from the AISA image do not correspond spatially with the ground truth measurements. High quality ortho-rectification, using a digital elevation model (DEM) of the same pixel size as the hyperspectral image, should be accomplished for elimination of this positioning error. Most effective option could be irreversible rectification, allowing to transform geocoded resampled hyperspectral image back to the original spectral form, as provided for instance by the PARGE software (Richter, 2005)

Recently, several authors reported that multi-directional and multi-angular remote sensing data are more sensitive to vegetation structure than NADIR data and therefore

can provide advanced structural descriptions of vegetation canopies (Chen, Liu et al., 2003; Schaepman, Koetz et al., 2005). The airborne AISA images of Bílý Kříž research site were acquired according to the multi-directional flight pattern. The exploration and the use of these data might improve the estimates of biophysical parameters (LAI) of this forest ecosystem.

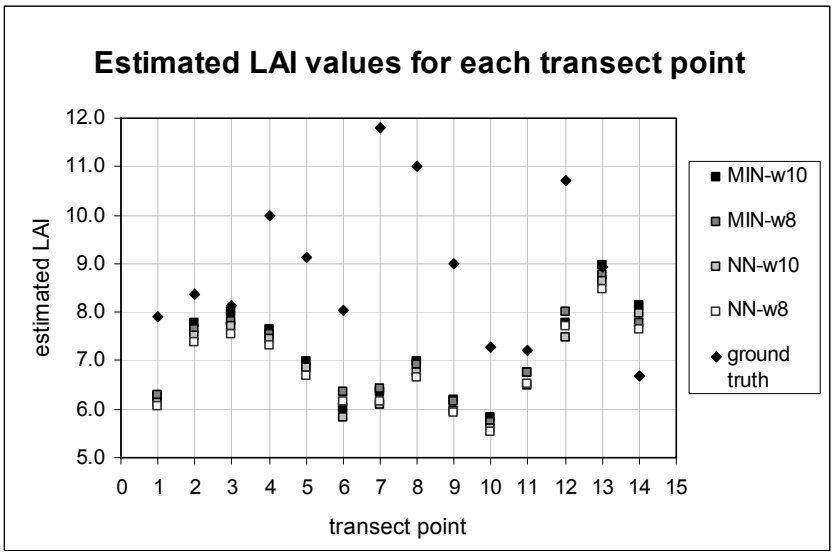

Figure 33. Estimated and measured values of LAI for each of the transect point used for the validation. (MIN = inversion of the LUT by the minimization cost function; NN = inversion of the LUT by the neural networks; w10 = sliding window of 10 m; w8 = sliding window of 8 m).

Table 13. Overview of the LAI retrieving methods performances by comparison with the field measurements of LAI (PCA-2000) after removing the outlaying values of transect points 7,8,9 and 12 (see figure 33).

Method	mean	R*	Sig.**	RMSE
Minimization cost function (window 10m)	7.23	0.292	0.412	1.478
Minimization cost function (window 8m)	7.15	0.337	0.341	1.460
Neural Networks (window 10m)	7.01	0.302	0.396	1.610
Neural Networks (window 8m)	6.93	0.331	0.350	1.616

* Pearson correlation coefficient; ** correlation is significant at the 0.01 level (2-tailed)

5.4.5. Comparison and evaluation of LAI inversion methods

From figure 30 and figure 33 is obvious that both inversion methods, no matter what extent of sliding window was used, gave very similar estimates, following the same trend. Neglected influence of the sliding window size is supported by the results of figure 31. The change in estimated LAI due to different window size is mostly +/- 1.5. Estimation carried out by 10m window size is giving only 0.014 higher LAI values in average than 8m window size estimation. However, dimension of the sliding window does affect the resultant LAI maps, and that is why its complete influence should be explored by including more window size variations. It is expected that especially larger

window extents (e.g. about 20-30m) could have stronger influence on the overall LAI prediction.

The inter-comparison of both LUT inversion methods, mentioned in table 12, showed clearly high similarity in their performances (Pearson correlation coefficients higher than 0.98 in all cases). Difference in predicted LAI maps of both inversion approaches ranges in general from 0.5 to -0.7. These results invoke a conclusion that both chosen inversion methods can fully substitute each other in LAI estimation from hyperspectral image of very high spatial resolution. Moreover, a type of the selected inversion approach seems to cause smaller inaccuracy in LAI estimation than selection of the involved spectral bands. Nevertheless, this hypothesis is speculative and needs to be verified by a further systematic research including new additional reflectance information or reflectance derived products (e.g. optical indices).

6. Conclusions and recommendations

An extensive literature review done by Pokorny (2002) reported the possible LAI values for Norway spruce stands ranging between 2 – 17 (Leverenz, Hinckley, 1990; Bartak, Dvorak et al., 1993). The destructive measurement of leaf area index conducted in 1997 at the research site Bílý Kříž, resulted into the value of 8.6 for leaf area index of the young forest stand (Pokorny, 2002). Regular temporal monitoring of leaf area index variability denotes the mean LAI values of 11.49 and 8.47 for dense and sparse part of the young Norway spruce forest stand measured by Pokorny (2005) during the growing period 2003. The mean LAI values of the whole stand of interest derived from the AISA image are 6.33 and 6.17 for the minimization approach inverting LUT and neural network approach, respectively. The retrieved values fit to the expected range of leaf area index values reported in literature, which could be taken as a proof of reliability of the inversion methods to estimate leaf area index of a young Norway spruce stand from NADIR hyperspectral data. On the other hand, the estimated values are in general lower than observed LAI values within the same stand. Moreover, the comparison of estimated LAI values with ground measurements showed very poor correlations, which indicates insufficient accuracy of the LAI estimates from the AISA image.

The ground-based measurements of leaf area index of the sample points, using Li-Cor PCA LAI-2000, indicated the range of the measured LAI values approximately between 6.5 - 12. In general the LAI values higher than 9 were not detected properly by none of the inversion methods. The results indicate that selected AISA spectral bands and/or the ratio between shaded and sunlit crown pixels are not the optimal indicators to estimate LAI from hyperspectral data. Therefore, it is recommended to include additional spectral bands (e.g. from red and SWIR part of spectra) or their derivatives to improve the current performances of the selected inversion methods. Also an additional image processing (e.g. automatic crown segmentation, or advanced AISA image orhorectification) should enhance accuracy of the LAI retrieval.

High Pearson correlation coefficients ($R > 0.98$) relating LAI estimates of both inverting approaches indicated no significant difference in their prediction accuracy. The minimization approach by a cost function could be evaluated as slightly better performing method than neural network approach based on comparison of the RMSE values computed between retrieved and measured LAI values (the mean RMSE = 2.442 for minimization approach while for NN the mean RMSE = 2.621). However, the difference is very small and so we can conclude that there is no significant difference in accuracy between selected inversion methods, operating at the level of a young Norway spruce forest stand.

Both of the inversion methods were inverting the spectral look-up tables generated from the RT simulations combined with the AISA image classification. The AISA image post-processing, a proper DART parameterization and building the look-up tables were more demanding and time-consuming procedures then both of the inversion

approaches. From this point of view, there is no feasibility difference between the selected inversion methods. The inversion of the look-up tables with the cost minimization function was fully automated, and whole procedure took about three hours. While the inversion procedure by means of artificial neural network method, using the ThinksPro software package, took more time. Establishment of the NN in ThinksPro required extensive testing of several NN architectures, training of the selected NN architecture for each canopy closure separately, and finally application of the trained NN. Based on this, the minimization approach by a cost function is considered to be more efficient, taking into account the input data, time and technical requirements. On the other hand, usage of more advanced neural network software may speed up the NN inversion process and even increase the result accuracy.

A performance evaluation of the Discrete Anisotropic Radiative Transfer (DART) model extended by the new structural features was not the main objective of this study. Our research only demonstrates feasibility of the DART parameterization, based purely on the field measurements of the Norway spruce structural characteristics. Nevertheless, several drawbacks were revealed during the DART parameterization process. Their revision and correction should improve performance of the next version of the DART model.

7. References

Allen, W. A., Gausman, H. W., et al. (1969). "Interaction of isotropic light with a compact plant leaf." J Opt Soc Amer 59(10): 1376-1379.

Anonymous (2004). Report on Forestry of the Czech Republic by December 31, 2003 (Zpráva o stavu lesa a lesního hospodárství Ceské republiky k 31.12.2003), Ministry of Agriculture of the Czech Republic.

Asner, G. P. (1998). "Biophysical and Biochemical Sources of Variability in Canopy Reflectance." Remote Sensing of Environment 64(3): 234-253.

Atzberger, C. (2004). "Object-based retrieval of biophysical canopy variables using artificial neural nets and radiative transfer models." Remote Sensing of Environment 93(1-2): 53-67.

Baret, F. and Guyot, G. (1991). "Potentials and limits of vegetation indices for LAI and APAR assessment." Remote Sensing of Environment 35(2-3): 161-173.

Baret, F. and Weiss, M. (2004). CAN_EYE: Processing digital photographs for canopy structure characterization, INRA, Avignon, France.

Baret, F., Weiss, M., et al. (2005). "VALERI: a network of sites and a methodology for the validation of medium spatial resolution land satellite products." not published (http://avignon.infra.fr/valeri/).

Bartak, M., Dvorak, V., et al. (1993). "Rozlozeni biomasy jehlic v korunove vrstve smrkoveho porostu." Lesnictivi - Forestry (Praha) 39(7): 247-281.

Borel, C. C., Gerstl, S. A. W., et al. (1991). "The radiosity method in optical remote sensing of structured 3-D surfaces." Remote Sensing of Environment 36(1): 13-44.

Bréda, N. J. J. (2003). "Ground-based measurements of leaf area index: a review of methods, instruments and current controversies." Journal of Experimental Botany 54: 2403-2417.

Broge, N. H. and Leblanc, E. (2001). "Comparing prediction power and stability of broadband and hyperspectral vegetation indices for estimation of green leaf area index and canopy chlorophyll density." Remote Sensing of Environment 76(2): 156-172.

Cape, J. N., Paterson, I. S., et al. (1989). "Regional variation in surface properties of Norway spruce and scots pine needles in relation to forest decline." Environmental Pollution 58(4): 325-342.

Chason, J. W., Baldocchi, D. D., et al. (1991). "A comparison of direct and indirect methods for estimating forest canopy leaf area." Agricultural and Forest Meteorology 57(1-3): 107-128.

Chen, J. M. (1996). "Optically-based methods for measuring seasonal variation of leaf area index in boreal conifer stands." Agricultural and Forest Meteorology 80(2-4): 135-163.

Chen, J. M. and Black, T. A. (1992). "Defining leaf area index for non-flat leaves." Plant, Cell & Environment 15(4): 421-429.

Chen, J. M. and Cihlar, J. (1996). "Retrieving leaf area index of boreal conifer forests using Landsat TM images." Remote Sensing of Environment 55(2): 153-162.

Chen, J. M., Li, X., et al. (2000). "Recent advances in geometrical optical modelling and its applications." Remote Sensing Reviews 18(2-4): 227-262.

Chen, J. M., Liu, J., et al. (2003). "Multi-angular optical remote sensing for assessing vegetation structure and carbon absorption." Remote Sensing of Environment 84(4): 516-525.

Chen, J. M., Rich, P. M., et al. (1997). "Leaf area index of boreal forests: Theory, techniques and measurements." Journal of Geophysical Research 102(D24): 29,429-29,443.

Colombo, R., Bellingeri, D., et al. (2003). "Retrieval of leaf area index in different vegetation types using high resolution satellite data." Remote Sensing of Environment 86(1): 120-131.

Combal, B., Baret, F., et al. (2003). "Retrieval of canopy biophysical variables from bidirectional reflectance: Using prior information to solve the ill-posed inverse problem." Remote Sensing of Environment 84(1): 1-15.

Combal, B., Baret, F., et al. (2002). "Retrieval of canopy biophysical variables from bidirectional reflectance using prior information to solve the ill-posed inverse problem." Remote Sensing of Environment 84(1): 1-15.

Cudlin, P., Novotny, R., et al. (2001). "Retrospective evaluation of the response of montane forest ecosystems to multiple stress." Ekologia Bratislava 20(1): 108-124.

Culvenor, D. S. (2002). "TIDA: an algorithm for the delineation of tree crowns in high spatial resolution remotely sensed imagery." Computers & Geosciences 28(1): 33-44.

Daughtry, C. S. T. (1989). "A new technique to measure the spectral properties of conifer needles." Remote Sensing of Environment 27(1): 81-91.

Dawson, T. P., Curran, P. J., et al. (1999). "The propagation of foliar biochemical absorption features in forest canopy reflectance: A theoretical analysis." Remote Sensing of Environment 67(2): 147-159.

Dawson, T. P., Curran, P. J., et al. (1998). "LIBERTY: Modeling the effects of leaf biochemical concentration on reflectance spectra." Remote Sensing of Environment 65(1): 50-60.

Demarez, V. and Gastellu-Etchegorry, J. P. (2000). "A Modeling Approach for Studying Forest Chlorophyll Content." Remote Sensing of Environment 71(2): 226-238.

Fang, H. and Liang, S. (2005). "A hybrid inversion method for mapping leaf area index from MODIS data: experiments and application to broadleaf and needleleaf canopies." Remote Sensing of Environment 94(3): 405-424.

Fang, H., Liang, S., et al. (2003). "Retrieving leaf area index using a genetic algorithm with a canopy radiative transfer model." Remote Sensing of Environment 85(3): 257-270.

Fassnacht, K. S., Gower, S. T., et al. (1994). "A comparison of optical and direct methods for estimating foliage surface area index in forests." Agricultural and Forest Meteorology 71(1-2): 183-207.

Ganapol, B. D., Johnson, L. F., et al. (1999). "LCM2: A coupled leaf/canopy radiative transfer model." Remote Sensing of Environment 70(2): 153-166.

Gascon, F., Gastellu-Etchegorry, J.-P., et al. (2004). "Retrieval of forest biophysical variables by inverting a 3-D radiative transfer model and using high and very high resolution imagery." International Journal of Remote Sensing 25(24): 5601-5616.

Gastellu-Etchegorry, J. P., Demarez, V., et al. (1996). "Modeling radiative transfer in heterogeneous 3-D vegetation canopies." Remote Sensing of Environment 58(2): 131-156.

Gastellu-Etchegorry, J. P., Guillevic, P., et al. (1999). "Modeling BRF and radiation regime of boreal and tropical forests: I. BRF." Remote Sensing of Environment 68(3): 281-316.

Gastellu-Etchegorry, J. P., Martin, E., et al. (2004). "DART: a 3D model for sumulating satellite images and studying surface radiation budget." Internation Journal of Remote Sensing 25: 73-96.

Gobron, N., Pinty, B., et al. (1997). "A semidiscrete model for the scattering of light by vegetation." Journal of Geophysical Research D: Atmospheres 102(8): 9431-9446.

Goel, N. S. and Grier, T. (1986). "Estimation of canopy parameters for inhomogeneous vegetation canopies from reflectance data. I. Two-dimensional row canopy." International Journal of Remote Sensing 7(5): 665-681.

Goel, N. S. and Grier, T. (1988). "Estimation of canopy parameters for inhomogeneous vegetation canopies from reflectance data: III. Trim: A model for radiative transfer in heterogeneous three-dimensional canopies." Remote Sensing of Environment 25(3): 255-293.

Gougeon, F. A. (1995). "A crown-following approach to the automatic delineation of individual tree crowns in high spatial resolution digital images." Canadian Journal of Remote Sensing 21: 274-284.

Gower, S. T., Kucharik, C. J., et al. (1999). "Direct and indirect estimation of leaf area index, fAPAR, and net primary production of terrestrial ecosystems." Remote Sensing of Environment 70(1): 29-51.

Gower, S. T. and Norman, J. M. (1991). "Rapid estimation of leaf area index in conifer and broad-leaved plantations." Ecology 72: 1896-1900.

Gruber, F. (1994). Morphology of coniferous trees: possible effects of soil acidification on the morphology of Norway spruce and Silver fir. Effects of acid rain on forest processes. D. Godbold and A. Hüttermann. New York, Wiley-Liss, Inc.

Haboudane, D., Miller, J. R., et al. (2004). "Hyperspectral vegetation indices and novel algorithms for predicting green LAI of crop canopies: Modeling and validation in the context of precision agriculture." Remote Sensing of Environment 90(3): 337-352.

Hall, R. J., Hogg, E. H., et al. (2003). "Relating aspen defoliation to changes in leaf area derived from field and satellite remote sensing data." Canadian Journal of Remote Sensing 29(3): 299-313.

Herman, F., Smidt, S., et al. (2001). "Evaluation of pollution-related stress factors for forest ecosystems in Central Europe." Environmental Science and Pollution Research 8(4): 231-242.

Hruska, J. and Cienciala, E., Eds. (2003). Long-term acidfication and nutrient degradation of forest soils - limiting factors of forestry today, Czech Ministry of Environment.

Hu, B., Inannen, K., et al. (2000). "Retrieval of leaf area index and canopy closure from CASI data over the BOREAS flux tower sites." Remote Sensing of Environment 74(2): 255-274.

IFER (2004). Field-Map. http://www.fieldmap.cz/

Jacquemoud, S. and Baret, F. (1990). "PROSPECT: A model of leaf optical properties spectra." Remote Sensing of Environment 34(2): 75-91.

Jacquemoud, S., Baret, F., et al. (1995). "Extraction of vegetation biophysical parameters by inversion of the PROSPECT + SAIL models on sugar beet canopy reflectance data. Application to TM and AVIRIS sensors." Remote Sensing of Environment 52(3): 163-172.

Jonckheere, I. (2004). "Review of mehtods for in situ leaf area index determination Part I. Theories, sensors and hemispherical pgotography." Agricultural and Forest Meteorology 121(1-2): 19-35.

Kimes, D., Gastellu-Etchegorry, J., et al. (2002). "Recovery of forest canopy characteristics through inversion of a complex 3D model." Remote Sensing of Environment 79(2-3): 320-328.

Kimes, D. S. and Kirchner, J. A. (1982). "Radiative transfer model for heterogeneous 3-D scenes." Applied Optics 21(22): 4119-4129.

Kraus, T., Broich, M., et al. (2005). LAI measurements in a tropical rainforest: Kakamega Forest, Kenya. http://www.avignon.inra.fr/valeri/

Kruse, F. A., Lefkoff, A. B., et al. (1993). "The spectral image processing system (SIPS)--interactive visualization and analysis of imaging spectrometer data." Remote Sensing of Environment 44(2-3): 145-163.

Kucharik, C. J., Norman, J. M., et al. (1998). "Measurements of leaf orientation, light distribution and sunlit leaf area in a boreal aspen forest." Agricultural and Forest Meteorology 91(1-2): 127-148.

Leckie, D. G., Gougeon, F. A., et al. (2005). "Automated tree recognition in old growth conifer stands with high resolution digital imagery." Remote Sensing of Environment 94(3): 311-326.

Lee, K.-S. (2004). "Hyperspectral versus multispectral data for estimating leaf area index in four different biomes." Remote Sensing of Environment 91(3-4): 508-520.

Leverenz, J. W. and Hinckley, T. M. (1990). "Shoot structure, leaf area index and productivity of evergreen conifer stands." Tree Physiology 6: 135-144.

Liang, S. (2004). Quantitative remote sensing of land surfaces. Hoboken, New Jersey, John Wiley & Sons, Inc.

LI-COR (1992). LAI-200 Plant Canopy Analyzer; Operating Manual.

Lillesand, T. M. and Kiefer, R. W. (2000). Remote Sensing and Image Interpretation (4th edition). New York, John Wiley & Sons, Inc.

Malenovský, Z., Cudlín, P., et al. (submitted). "Applicability of the PROSPECT model for Norway spruce needles." Internation Journal of Remote Sensing.

Malenovsky, Z., Martin, E., et al. (2003). Heterogeneity description improvements of spruce crown architecture simulated using the RD radiative transfer model DART. Proceedings of 2nd SPECTRA Workshop. ESA-ESTEC, Noordwijk, The Netherlands.

Martin, E. (2005). Evaluation of DART performaces: comparison of simulated BRF with measured BRF on AISA imagery, Personal communication.

Meer van der, F. D. and Jong de, S. M. (2001). Imaging Spectrometry: Basic Principles and Prospective Applications. Dordrecht, The Netherlands, Kluwer Academic Publishers.

Meroni, M., Colombo, R., et al. (2004). "Inversion of a radiative transfer model with hyperspectral observations for LAI mapping in poplar plantations." Remote Sensing of Environment 92(2): 195-206.

Mesarch, M. A., Walter-Shea, E. A., et al. (1999). "A Revised Measurement Methodology for Conifer Needles Spectral Optical Properties: Evaluating the Influence of Gaps between Elements." Remote Sensing of Environment 68(2): 177-192.

Monsi, M. and Saeki, T. (1953). "Uber den Lichtfaktor in den Pflanzengesellschaften und seine Bedeutung fur die Stoffproduktion." Japanese Journal of Botany 14: 22-52.

Nikolov, N. and Zeller, K. F. (2003). "Modeling coupled interactions of carbon, water, and ozone exchange between terrestrial ecosystems and the atmosphere. I: Model description." Environmental Pollution 124(2): 231-246.

Persson, Å., Holmgren, J., et al. (2002). "Detecting and measuring individual trees using an airborne laser scanner." Photogrammetry Engineering & Remote Sensing 68(9): 925-932.

Pinty, B., Gobron, N., et al. (2000). "The Radiation transfer Model Intercomparision (RAMI) Exercise." Journal of Geophysical Research 106(IWMMM - 2 Special issue): 11937-11956.

Pokorny, R. (2002). Index listove plochy v porostech lesnich drevin. Lesnicka a drevarska fakulta. Brno, Mendelova zemedelska a lesnicka univerzita**:** 135.

Pokorny, R. (2005). Long-term monitoring of leaf area index in dense and sparse canopies of the young Norway spruce forest stand, Presonal communication.

Pokorny, R. and Marek, M. V. (2000). "Test of accuracy of LAI estimation by LAI-2000 under artificially changed leaf to wood area proportions." Biologia Plantarum 43(4): 537-544.

Rautiainen, M., Stenberg, P., et al. (2004). "The effect of crown shape on the reflectance of coniferous stands." Remote Sensing of Environment 89(1): 41-52.

Rich, P. M., Clark, D. B., et al. (1993). "Long-term study of solar radiation regimes in a tropical wet forest using quantum sensors and hemispherical photography." Agricultural & Forest Meteorology 65(1-2): 107-127.

Richter, R. (2005). Atmospheric / Topographic Correction for Airborne Imagery (ATCOR-4 User Guide). Wessling (Germany), DLR - German Aerospace Center.

Roberts, S. D., Dean, T. J., et al. (2005). "Estimating individual tree leaf area in loblolly pine plantations using LiDAR-derived measurements of height and crown dimensions." Forest Ecology and Management In Press, Corrected Proof.

Schaepman, M. E., Koetz, B., et al. (2005). "Spectrodirectional remote sensing for the improved estimation of biophysical and -chemical variables: two case studies." International Journal of Applied Earth Observation and Geoinformation 6(3-4): 271-282.

Smith, N. J., Chen, J. M., et al. (1993). "Effects of clumping on estimates of stand leaf area index using the Li-Cor LAI-2000." Canadian Journal of Forest Research 23: 1940-1943.

SPECIM (2004). http://www.specim.fi/products-aisa-eagle.html

Stenberg, P. (1996). "Correcting LAI-2000 estimates for the clumping of needles in shoots of conifers." Agricultural and Forest Meteorology 79(1-2): 1-8.

Tian, Y., Wang, Y., et al. (2003). "Radiative transfer based scaling of LAI retrievals from reflectance data of different resolutions." Remote Sensing of Environment 84(1): 143-159.

Treitz, P. and Howarth, P. (1999). "Hyperspectral remote sensing for estimating biophysical parameters of forest ecosystems." Progress in Physical Geography 23(3): 359-390.

Ufer Gil, C. M. (2004). Comparison of scaling-up methods to retrive chlorophyll content in Norway spruce crowns from hyperspectral images simulated by the DART model. Laboratory of Geo-Information Science and Remote Sensing. Wageningen, Wageningen University and Research Centre**:** 73.

Verhoef, W. (1984). "Light scattering by leaf layers with application to canopy reflectance modeling: The SAIL model." Remote Sensing of Environment 16(2): 125-141.

Watson, D. J. (1974). "Comparative physiological studies in the growth of field crops I. Variation in net assimilation rate and leaf area between species and varieties, and within and between years." Annals of Botany 11: 41-76.

Weiss, M. (2004). "Review o fmethods for in situ leaf area index (LAI) determination Part II. Estimation of LAI, errors and sampling." Agricultural and Forest Meteorology 121(1-2): 37-53.

Wilson, J. W. (1960). "Inclined point quadrats." New Phytol 59: 1-8.

Zarco-Tejada, P. J., Miller, J. R., et al. (2004). "Needle chlorophyll content estimation through model inversion using hyperspectral data from boreal conifer forest canopies." Remote Sensing of Environment 89(2): 189-199.

Zimble, D. A., Evans, D. L., et al. (2003). "Characterizing vertical forest structure using small-footprint airborne LiDAR." Remote Sensing of Environment 87(2-3): 171-182.

8. Appendix

Appendix 1. The overview of the combinations of canopy closure (CC) and leaf volume density (u_f) simulated by the DART model and used to build the LUT database. Different combination of u_f and CC gave different leaf area index value of the simulated scenes, which is shown in the table.

u_f [m^2/m^3]	95%	90%	85%	75%	65%	55%	u_f [m^2/m^3]	95%	90%	85%	75%	65%	55%
0.8	1.5	1.3					**6.5**		10.7	9.7			
1	1.9	1.7	1.5	1.3			**6.6**	12.4	10.9	9.8	8.6	7.6	6.3
1.2	2.3	2.0	1.8				**6.7**		11.1	10.0			
1.4	2.6	2.3	2.1				**6.8**	12.8	11.2	10.1	8.9	7.8	6.5
1.5				2.0	1.7	1.4	**6.9**		11.4	10.3			
1.6	3.0	2.6	2.4				**7**	13.2	11.6	10.4	9.1	8.0	6.7
1.7							**7.1**		11.7	10.6			
1.8	3.4	3.0	2.7				**7.2**	13.5	11.9	10.7	9.4	8.3	6.9
1.9							**7.3**			10.9			
2	3.8	3.3	3.0	2.6	2.3	1.9	**7.4**	13.9	12.2	11.0	9.6	8.5	7.1
2.1	4.0						**7.5**			11.2			
2.2	4.1	3.6	3.3				**7.6**	14.3	12.6	11.3	9.9	8.7	7.3
2.3	4.3						**7.7**			11.4			
2.4	4.5	4.0	3.6				**7.8**	14.7	12.9	11.6	10.2	9.0	7.4
2.5	4.7	4.1		3.3	2.9	2.4	**7.9**			11.7			
2.6	4.9	4.3	3.9				**8**	15.1	13.2	11.9	10.4	9.2	7.6
2.7	5.1	4.5	4.0				**8.1**						
2.8	5.3	4.6	4.2				**8.2**		13.6	12.2	10.7	9.4	7.8
2.9	5.5	4.8	4.3				**8.3**						
3	5.6	5.0	4.5	3.9	3.4	2.9	**8.4**		13.9	12.5	10.9	9.7	8.0
3.1	5.8	5.1	4.6				**8.5**				11.1	9.8	8.1
3.2	6.0	5.3	4.8	4.2			**8.6**		14.2	12.8	11.2	9.9	8.2
3.3	6.2	5.5	4.9				**8.7**				11.3	10.0	8.3
3.4	6.4	5.6	5.1	4.4			**8.8**		14.6	13.1	11.5	10.1	8.4
3.5	6.6	5.8	5.2		4.0	3.3	**8.9**				11.6	10.2	8.5
3.6	6.8	6.0	5.4	4.7			**9**		14.9	13.4	11.7	10.3	8.6
3.7	7.0	6.1	5.5				**9.1**					10.5	8.7
3.8	7.2	6.3	5.7	4.9	4.4		**9.2**			13.7		10.6	8.8
3.9	7.3	6.4	5.8				**9.3**						
4	7.5	6.6	5.9	5.2	4.6	3.8	**9.4**			14.0		10.8	9.0
4.1	7.7	6.8	6.1				**9.5**				12.4		
4.2	7.9	6.9	6.2	5.5	4.8	4.0	**9.6**			14.3		11.0	9.2
4.3	8.1	7.1	6.4				**9.8**			14.6		11.3	9.4
4.4	8.3	7.3	6.5	5.7	5.1	4.2	**10**			14.9	13.0	11.5	9.5
4.5	8.5	7.4	6.7				**10.2**					11.7	9.7
4.6	8.7	7.6	6.8	6.0	5.3	4.4	**10.4**						9.9
4.7	8.8	7.8	7.0				**10.5**				13.7	12.1	
4.8	9.0	7.9	7.1	6.3	5.5	4.6	**10.6**						10.1
4.9	9.2	8.1	7.3				**10.8**						10.3
5	9.4	8.3	7.4	6.5	5.7	4.8	**11**				14.3	12.6	10.5
5.1	9.6	8.4	7.6				**11.2**						10.7
5.2	9.8	8.6	7.7	6.8	6.0	5.0	**11.4**						10.9
5.3	10.0	8.8	7.9				**11.5**				15.0	13.2	
5.4	10.2	8.9	8.0	7.0	6.2	5.2	**11.6**						11.1
5.5	10.3	9.1	8.2				**11.8**						11.3
5.6	10.5	9.3	8.3	7.3	6.4	5.3	**12**					13.8	11.4
5.7	10.7	9.4	8.5				**12.2**						11.6
5.8	10.9	9.6	8.6	7.6	6.7	5.5	**12.5**					14.4	11.9
5.9	11.1	9.8	8.8				**13**					14.9	12.4
6	11.3	9.9	8.9	7.8	6.9	5.7	**13.5**						12.9
6.1	11.5	10.1	9.1				**14**						13.4
6.2	11.7	10.3	9.2	8.1	7.1	5.9	**14.5**						13.8
6.3	11.9	10.4	9.4				**15**						14.3
6.4	12.0	10.6	9.5	8.3	7.4	6.1	**15.5**						14.8

Appendix 2. The extracted spectral characteristics from the DART outputs for the simulated AISA spectral bands no. 37, 38 and 40. The left column of graphs presents the overall reflectance (BRF) of the simulated canopy closure scenes. The right column of graphs presents spectral characteristics extracted for shaded and sunlit part of Norway spruce crowns.

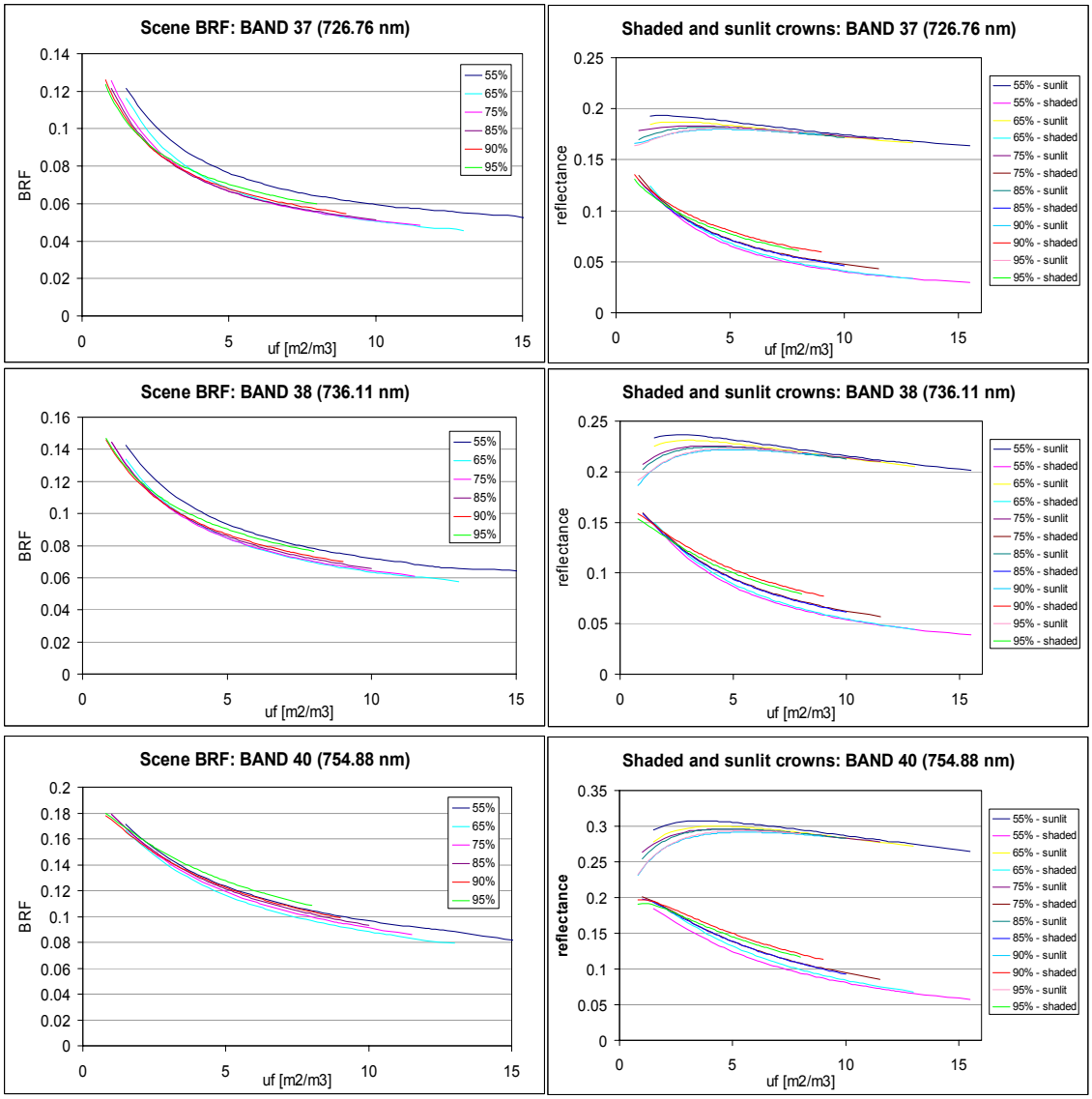

Appendix 3. The ratios, used to build the spectral LUT database, between shaded and sunlit parts of crowns derived for each canopy closure category, calculated for the AISA spectral bands no. 37, 38 and 40.